

Melt inclusion constraints on mantle carbon heterogeneity within an individual mantle plume and at the global scale

Simon Matthews^{a,*}, Oliver Shorttle^{a,b}, John MacLennan^a, John F. Rudge^a

^a*Department of Earth Sciences, University of Cambridge, Downing Street, Cambridge, CB2 3EQ, UK.*

^b*Institute of Astronomy, University of Cambridge, Madingley Road, Cambridge, CB3 0HA, UK.*

Abstract

The Earth's mantle holds more carbon than its oceans, atmosphere and continents combined, yet the distribution of carbon within the mantle remains uncertain. Global variations in the carbon content of the depleted mantle have been inferred from carbon-trace element systematics of ultra-depleted mid-ocean ridge glasses and melt inclusions, though the origin of mantle carbon variability remains uncertain. A variety of observations suggest that the mantle plumes underlying ocean islands have high bulk carbon contents, but the characterisation of individual mantle plume components has not been possible.

We supplement the existing melt inclusion data from Iceland with four new datasets, significantly enhancing the spatial and geochemical coverage. Within the combined dataset there is significant variation in melt inclusion CO₂/Ba ratio, which is tightly correlated with trace element enrichment. The trends in CO₂/Ba–Ba space displayed by our new data coincide with the same trends in data compiled from global ocean islands and mid-ocean ridges, forming a global array. The overall structure of the global CO₂/Ba array is not a property of the source, instead controlled by CO₂ degassing before melt inclusion entrapment, and CO₂ loss by decrepitation following inclusion entrapment.

The position of melt inclusion datasets within the global array allows us to filter out inclusions likely to have undergone decrepitation. Providing earlier CO₂ degassing and magma mixing have not destroyed the mantle signal, the remaining inclusions may preserve mantle CO₂/Ba values. Using the observed covariation of the filtered CO₂/Ba ratio with radiogenic isotope tracers of mantle source, we find CO₂ concentrations in the Icelandic depleted mantle of 102^{+53}_{-27} ppmw, typical of mantle underlying the mid-ocean ridge system, and high CO₂ concentrations of $2.2^{+3.8}_{-1.5}$ wt% associated with the high ³He/⁴He component of the Iceland plume. However, source and process are difficult to deconvolve for the eruptions most sensitive to enriched, or recycled, mantle components; the presently available data is consistent with recycled material being either enriched or depleted in carbon.

Extending our approach globally, we find no systematic variation in CO₂/Ba or CO₂/Nb with enrichment (in the absence of a primordial mantle contribution). The lack of global co-variation suggests mechanisms recycling CO₂ from the surface into the convecting mantle are decoupled from those recycling most trace elements. However, the variation of CO₂/Nb with Ba/Nb suggests Ba may behave similarly to CO₂ during recycling.

Keywords: Mantle, Carbon, Heterogeneity, Iceland, Melt Inclusions, Recycling, Primordial

1. Introduction

The majority of Earth's carbon, that has not been sequestered to the core, resides in the mantle (Dasgupta and Hirschmann, 2010; Kelemen and

Manning, 2015). Carbon exchange between the surface and deep occurs principally by volcanic outgassing and subduction of oceanic plates. Since the advent of plate tectonics these processes have shaped the inventories of carbon within the surface and mantle reservoirs. However, the magnitude of these fluxes, both at the present day and in

*Now at Department of Earth and Planetary Sciences, Johns Hopkins University, Baltimore, MD 21218, USA. simonmatthews@jhu.edu

the Earth’s deep past, remain largely uncertain. A great deal of this uncertainty is associated with the efficiency of carbon recycling in subducting slabs; thermodynamic modelling suggests slab decarbonation should be limited in most subduction zones (Kerrick and Connolly, 2001), but the infiltration of hydrous fluids may mobilise carbonate from the subducting plate (Kelemen and Manning, 2015). Hirschmann (2018) placed empirical bounds on recycling efficiency by comparing the CO_2/Ba ratios of the Earth’s exosphere and upper mantle and found that at least 25%, and probably much more, of the carbon outgassed to the exosphere must have been returned to the mantle via subduction.

An alternative, but complementary, approach to constraining CO_2 recycling efficiency is to estimate the amount of carbon within recycled mantle domains where they are sampled at ocean islands. CO_2 -noble gas systematics of fluid inclusions in material erupted in Hawaii and La Réunion Island indicate their mantle sources are carbon rich (Trull et al., 1993; Boudoire et al., 2018), which is further supported by models that couple CO_2 emission rates with magma supply rates at Hawaii (Anderson and Poland, 2017) and high CO_2 contents of primitive melts (Tucker et al., 2019). However, both Hawaii and La Réunion are underlain by mantle plumes transporting primordial (high $^3\text{He}/^4\text{He}$) mantle, which may contain high concentrations of carbon (Miller et al., 2019). In order to assess the efficiency of carbon recycling it is necessary to deconvolve the contributions of carbon from recycled and primordial mantle domains to volcanic outgassing.

Progress in identifying mantle carbon variability has been hampered by its tendency to exsolve from magmas into a CO_2 vapour phase. The solubility of CO_2 in basaltic melts is minimal at the low pressures of eruption (Stolper and Holloway, 1988), with the consequence that considerable CO_2 will have been lost by CO_2 vapour exsolution (degassing) in all but the most CO_2 poor melts.

1.1. Estimating mantle carbon

A number of approaches have been taken to circumvent the overprint of degassing on the mantle CO_2 signals. Rare ultra-depleted glasses erupted in oceanic fracture zones often contain sufficiently low concentrations of CO_2 that they are undersaturated in CO_2 vapour at the pressure of eruption. However, Matthews et al. (2017) suggested these magmas formed by mixing of trace-element and

CO_2 enriched melts that are partially degassed with trace-element and CO_2 depleted melts; with the significant CO_2 vapour undersaturation of the depleted melts conferring CO_2 undersaturation onto the mixed magma. This process is difficult to definitively identify and could lead to underestimates of mantle CO_2 concentrations. Occasionally, extremely trace-element enriched mid-ocean ridge basalt (MORB) glasses retain gas rich vesicles, which may contain the full budget of CO_2 and other volatiles that exsolved from the magma (Cartigny et al., 2008; Jones et al., 2019). It is again unclear whether these enriched magmas lost CO_2 deeper within the crust, before beginning to retain vesicles. Furthermore, the MORB glass datasets only provide information about the mantle underlying the mid-ocean ridge system and are therefore biased towards characterising the depleted upper mantle.

Another approach uses melt inclusions, tiny droplets of magma trapped within crystals as they grow at depth within the crust. The elastic strength of the host crystals prevents decompression of the inclusion to the pressure of the surrounding melt, potentially allowing the melt to remain undersaturated in CO_2 vapour. Not only are melt inclusions ubiquitous in MORB, but they can also be readily found in ocean island basalt (OIB). Melt inclusions also offer an unrivalled view of the earliest stages of magma evolution, when the diversity of melt chemistry generated by near-fractional melting is still partially preserved (Sobolev and Shimizu, 1993). However, the CO_2 budget of melt inclusions remains susceptible to the same degassing and mixing processes as the ultra-depleted glasses. Post-entrapment CO_2 loss via decrepitation of the host crystals is also likely to occur (MacLennan, 2017).

1.2. Ratios of CO_2 and trace-element concentrations

One process affecting carbon that it may be possible to successfully control for is melting. Ratios of CO_2 to Ba or Nb concentrations have been used to achieve this (Saal et al., 2002; Le Voyer et al., 2017; Hauri et al., 2018; Michael and Graham, 2015; Shimizu et al., 2016; Tucker et al., 2019; Shimizu et al., 2019; Miller et al., 2019), since CO_2 , Ba, and Nb partition similarly during mantle melting (Saal et al., 2002; Rosenthal et al., 2015). Given this similarity in partitioning behaviour, it should be expected that pre-degassing magmatic values of CO_2/Ba and CO_2/Nb will not be fractionated from

their mantle sources; the exception to this being that even small differences between the partition coefficients can cause large variations in the CO_2/Ba and CO_2/Nb of instantaneous fractional melts extracted from a previously depleted source (Rosenthal et al., 2015).

A number of previous studies (Saal et al., 2002; Le Voyer et al., 2017; Hauri et al., 2018) are predicated upon correlations between CO_2 and Ba or Nb indicating a lack of any fractionation between CO_2 and the incompatible trace elements, including the absence of any CO_2 degassing prior to, or after, inclusion entrapment. However, Matthews et al. (2017) demonstrated that such correlations are also a natural consequence of degassing and mixing of compositionally diverse near-fractional mantle melts, and such a process can explain the increasing variation in CO_2/Ba with Ba concentration that many datasets exhibit.

Magma mixing is common in magmatic systems (Sobolev, 1996; MacLennan, 2008a; Shorttle, 2015; Shorttle et al., 2016), and the most CO_2 rich fractional melts are expected to saturate in CO_2 vapour at pressures within, or below, the crust (Dixon et al., 1995). Though the degassing and mixing process causes the average value of CO_2/Ba within a dataset to be controlled primarily by the pressure of degassing, the maximum values seen in a dataset may still record the mantle value (or are at least a minimum estimate of the mantle value). Datasets that do not exhibit correlations likely have a more complex multi-stage degassing history, making them less reliable records of mantle CO_2/Ba ratios.

Shimizu et al. (2019) recently demonstrated that not all melt inclusion datasets require a partial-degassing and mixing process to explain their CO_2 -trace element systematics. For inclusions from the Siqueiros and Garrett transform faults, Shimizu et al. (2019) showed that the covariance of CO_2 with a broad suite of trace elements is compatible with the trapped melts having a single mantle-derived CO_2/Ba ratio for variable Ba concentration. The observed variability in CO_2/Ba and CO_2/Nb ratios arises from analytical imprecision. However, partially degassed datasets can also give rise to melt inclusions with a single CO_2/Ba ratio at variable Ba concentration. If the trace-element and CO_2 enriched melts degas, but are then efficiently homogenised, a single enriched mixing endmember is produced, with a CO_2/Ba ratio lower than the mantle value (Matthews et al., 2017, Appendix A).

When mixed with extremely trace-element and CO_2 depleted melts, a binary mixing array in CO_2 -Ba space will be generated with each melt having an identical CO_2/Ba ratio. In this scenario, the mean CO_2/Ba ratio of the datasets would then be only a minimum bound on the mantle value. The implications and likelihood of such a process for the Siqueiros and Garrett datasets are discussed in Section 5.7.

To understand what CO_2/Ba and CO_2/Nb ratios tell us about mantle carbon heterogeneity we need to consider how these elements are transferred to the melt. During mantle melting, the residue is likely to be completely depleted of CO_2 after only a few percent melting, either by the formation of carbonatitic or carbonated-silicate melts if a carbon phase is present (Dasgupta and Hirschmann, 2010), or by virtue of the incompatibility of CO_2 in silicate minerals (Saal et al., 2002; Rosenthal et al., 2015). Even refractory mantle lithologies are likely to have entirely lost their carbon to a melt phase long before silicate melting begins. Since such low-degree melts have a vanishingly small chance of escaping mixing during transport, we assume that melts in one location will not preserve the variable CO_2/Ba and CO_2/Nb ratios of small-scale heterogeneities, but instead will inherit an average value. Larger scale variations in the relative proportions of small-scale heterogeneities may allow the relative contributions of different mantle components to the CO_2 budget of the magma to be deconvolved.

1.3. Identifying mantle CO_2 heterogeneity

In this contribution we seek to assess the presence of carbon rich mantle reservoirs in the Earth. In order to deconvolve the signals of CO_2 degassing and mantle heterogeneity, a large number of melt inclusions from eruptions sampling a diversity of mantle sources need to be analysed for both their trace element and CO_2 concentrations. We approach this by considering mantle carbon heterogeneity on the scale of both a single well sampled mantle plume (Iceland), and a global scale with the more sparsely sampled mid-ocean ridges and ocean islands. Iceland offers an excellent opportunity for studying carbon heterogeneity within a single mantle plume due to the large number of previous melt inclusion studies (Hauri et al., 2018; Hartley et al., 2014; Neave et al., 2014; Bali et al., 2018; Schipper et al., 2016; Miller et al., 2019), which we supplement with four new datasets (Sections 2 and Section 3.1).

Comparisons between the CO₂-trace element systematics present within the Iceland melt inclusion compilation and the global compilation enable us to make a new assessment of the effects of crustal storage and melt inclusion decrepitation (Section 4). Though this secondary crustal processing signal dominates the global CO₂/Ba and CO₂/Nb arrays, in Section 5 we demonstrate that a signal of mantle source CO₂ heterogeneity still remains in the Iceland compilation. By inversion of a three component mixing model (Section 5.4) we estimate CO₂ concentrations, and their uncertainties, in endmember mantle components within the Iceland plume. We find evidence that CO₂ concentrations higher than in the depleted mantle are present within the primordial mantle, and lower in recycled mantle (though poorly constrained).

2. Samples and Methods

Samples were collected from four fresh primitive eruptions in Iceland (Figure 1) which represent diverse mantle sources, as indicated by their Sr-, Nd- and He-isotope ratios. Háleyjabunga and Stapafell are in close proximity on the Reykjanes Peninsula in the Western Rift Zone, but preferentially sample more depleted and enriched mantle components respectively (Thirlwall et al., 2004). Stapafell erupted sub-glacially between 70 and 14 ka (Saemundsson et al., 2010) forming basal pillow basalts, from which samples were taken near 63°54.585'N, 22°31.409'W. Háleyjabunga was erupted as a sub-aerial lava shield at ~13 ka (Saemundsson et al., 2010), from which olivine-phyric lava flow samples were taken from the Eastern side of the vent near 63°48.978'N, 22°39.099'W. Berserkjahraun is an eruption younger than 11 ka in the Snæfellsnes flank zone (Hjartarson and Sæmundsson, 2014), and has extreme geochemical enrichment (Peate et al., 2010). Glassy olivine- and plagioclase-phyric scoria was collected from the crater at 64°95.915'N, 22°89.853'W. Heilagsdalsfjall is a lava flow erupted in the Northern Volcanic Zone with an age < 11.5 ka (Sæmundsson et al., 2012). Glassy olivine-phyric achneliths were collected from the crater at 65.49934°N, 16.70224°W.

Olivine and clinopyroxene crystals containing melt inclusions were extracted from each sample. The total CO₂ content of a melt inclusion is partitioned between the glass and vapour bubble (if present). Following Hartley et al. (2014), crystals

were sequentially prepared for micro-Raman analysis of CO₂ vapour density in the bubbles, Secondary Ion Mass Spectrometry (SIMS) to determine CO₂ and trace element concentrations in the glass, and electron probe microanalysis (EPMA) to determine the major element chemistry of the inclusions and their crystal hosts. Any CO₂ detected in the inclusion-hosted bubbles was added back into the glass, assuming the inclusion was a homogeneous melt phase at the time of entrapment. Full information on sample preparation and analytical setup is given in the Supplementary Information. In Appendix A we explain why we do not apply a correction based on predicting the CO₂ vapour density in bubbles. As we are primarily interested in trace element ratios, and CO₂ concentrations at the time of eruption, we do not apply post-entrapment crystallisation corrections (though we provide sufficient information in Supplementary Tables that this may be performed).

3. Results

The four new datasets from Berserkjahraun, Háleyjabunga, Heilagsdalsfjall, and Stapafell are described in Section . In Section 3.2 we consider our new datasets alongside others from Iceland to assess whether the mantle CO₂/Ba ratio has survived the melting process. Finally, we discuss the processes most likely to be controlling the CO₂-trace element systematics (Section 3.3).

3.1. CO₂ and trace elements

Melt inclusion CO₂ and Ba concentrations, with and without bubble corrections, are shown for each eruption in Figure 2. All four eruptions show considerable variation in their CO₂/Ba ratios, but only Háleyjabunga and Stapafell display positive correlations between CO₂ and Ba. Only three Háleyjabunga melt inclusions analysed by SIMS contained bubbles in which CO₂ vapour was detected (a further three were measured by Raman only, as shown in Supplementary Figure 1d). Though five Stapafell melt inclusion hosted bubbles contained CO₂ vapour (Supplementary Figure 1e), only one was in an inclusion analysed by SIMS. No CO₂ vapour was detected in any of the bubbles hosted in Heilagsdalsfjall inclusions. A substantial fraction of Berserkjahraun inclusions contained bubbles in which CO₂ vapour was detected. In Háleyjabunga, Stapafell and Berserkjahraun, the highest CO₂ concentrations are in inclusions where corrections have

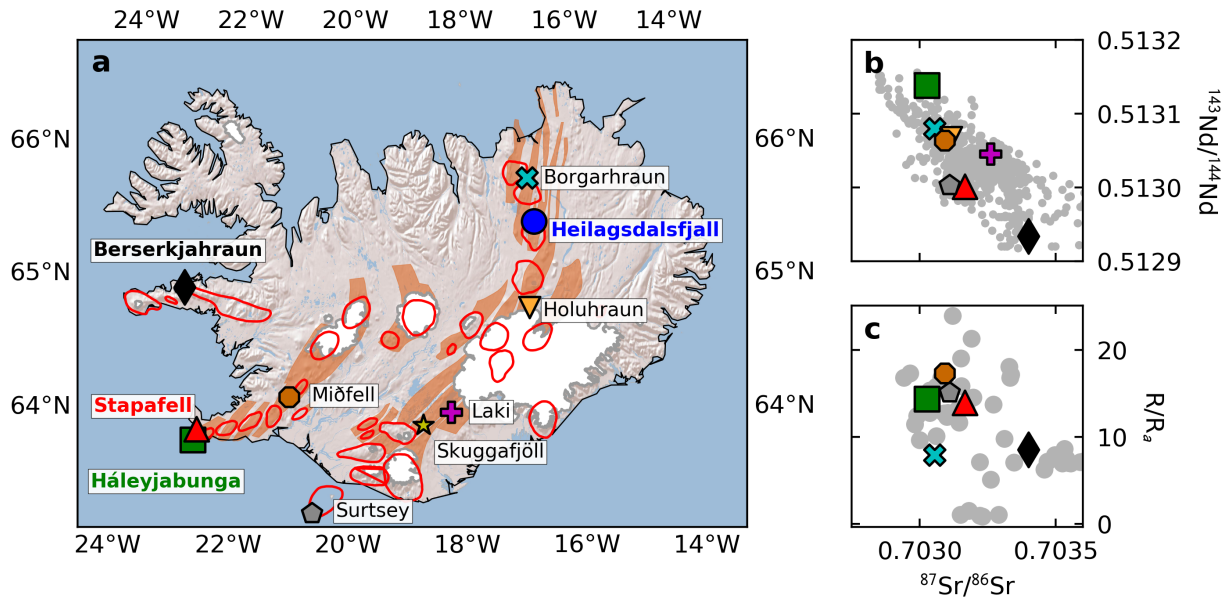


Figure 1: Panel a: Locations of the eruptions studied here (bold text and large symbols), and the locations of other Icelandic eruptions for which CO_2 and trace element measurements have been made on melt inclusions. Orange shading shows the active rift zones. Red outlines show active volcanic centres. Panel b: Sr and Nd isotope ratios of whole rocks from the same eruptions. Panel c: $^3\text{He}/^4\text{He}$ isotope ratio (R) normalised to the atmospheric value (R_a). Grey circles in panels b and c show data compiled for Iceland (sources given in Supplementary Information). Isotope data not available for Skuggafjöll and Heilagsdalsfjall.

been applied. For Háleyjabunga and Stapafell, the corrected inclusions do not have higher CO_2/Ba than uncorrected inclusions. However, the corrections applied to the Berserkjahraun inclusions are extremely large and consequently significantly increase the CO_2/Ba ratios recorded by the melt inclusion population. The large magnitude of the corrections arises from high CO_2 vapour densities up to 0.75 g cm^{-3} . Though this density is above the maximum density of vapour in coexistence with liquid CO_2 at room temperature ($\sim 0.13 \text{ g cm}^{-3}$), any heating by the Raman instrument's laser could move the bubble beyond the CO_2 triple point. The bubble volume fraction exerts some control on the corrected CO_2 concentration, but little dependence on CO_2 vapour density is observed (Supplementary Figure 2). A sub-population of three Háleyjabunga melt inclusions have much higher (bubble-uncorrected) CO_2 concentrations than the general population (distinguished on Figures 2 and 3), the origin of this feature is discussed further in Section 3.3.

Trace element concentrations in the four melt inclusion suites are shown in Figure 3. Melt inclusions from Háleyjabunga (Figure 3a) show ex-

treme variability in relative trace element enrichment, MacLennan (2008b) and Neave et al. (2018) argued this variability is most likely mantle derived. The Háleyjabunga matrix has a depleted trace element pattern (Skovgaard et al., 2001). Four Háleyjabunga inclusions have anomalously high Ba and Nb concentrations relative to the light rare earth elements; since their CO_2 concentrations are similar to the main population of inclusions they have not retained high CO_2/Ba or CO_2/Nb ratios. The Háleyjabunga inclusion with highest CO_2/Ba ratio is part of the high- CO_2 population, but as we discuss in Section 3.3 this may not reflect a mantle value, and so we treat this inclusion as an anomaly here. Ignoring this anomalous inclusion, the highest CO_2/Ba ratios (>200) are observed in inclusions with depleted trace element patterns, but are not anomalously depleted among the larger population of Háleyjabunga inclusions.

The Stapafell inclusions with highest CO_2/Ba (Figure 3b) show trace element patterns with anomalously low Ba and Nb concentrations relative to the light and middle rare earth elements. Despite the anomalous trace element patterns of a small number of Stapafell inclusions, Ba, Nb and CO_2

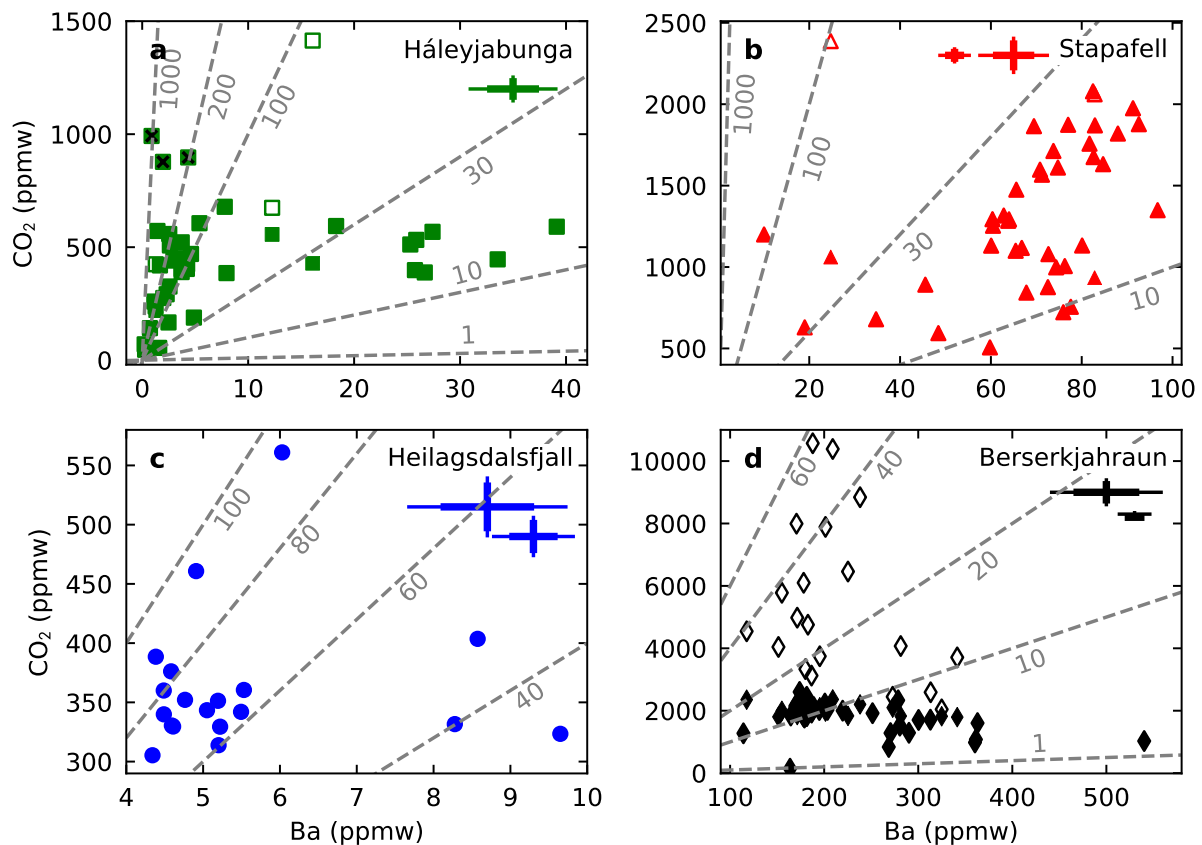


Figure 2: Melt inclusion glass (filled symbols) and reconstructed (open symbols) CO_2 concentrations plotted against Ba concentration for each of the four eruptions studied here. The dashed grey lines indicate constant CO_2/Ba ratio. In panel a (Háleyjabunga), the three inclusions thought to represent a different population, as discussed in the main text, are highlighted with black crosses. Error bars show typical uncertainties for enriched (large error bars), and depleted (small error bars) melt inclusion analyses in each eruption. The bold lines show the estimated 1 s.d. precision, and thin lines show 1 s.d. combined precision and accuracy. The uncertainties for the depleted Háleyjabunga inclusions are smaller than the symbols.

appear to be unfractionated from each other, discussed further in Section 3.2. The Stapafell melt inclusions show enriched trace element patterns, and our new observations are consistent with the conclusions of Neave et al. (2018) that the variability is not mantle derived, but largely reflects variable crystal fractionation.

The Heilagsdalsfjall melt inclusions (Figure 3c) show little trace element variability, and have a strong depleted mantle signature. Berserkjähraun melt inclusions (Figure 3d) show the most extreme enriched signatures of the four eruptions, and show little mantle-derived variability among the inclusions. The small Sr- and Zr-anomalies seen in many of the inclusions from all four eruptions are likely the result of interaction with plagioclase in the crust (Aigner-Torres et al., 2007).

3.2. Fractionation of Ba, Nb and CO₂ during melting

Primary magmas will only preserve mantle CO₂/Ba and CO₂/Nb ratios if Ba, Nb and CO₂ are not fractionated from each other during mantle melting. Crustal processes are not expected to fractionate Ba from Nb, but magma degassing will cause CO₂ to be fractionated from both. The melt inclusions least affected by degassing can be identified by taking the highest CO₂/Ba ratios (Matthews et al., 2017).

However, neither this filtering process, nor observations of the distribution of CO₂-trace element ratios, can conclusively rule out small degrees of fractionation of CO₂ from Ba and Nb during melting. Experimental work by Rosenthal et al. (2015) suggests that during mantle melting CO₂ should behave marginally more compatibly than Ba, and less compatibly than Nb. Therefore, if Nb and Ba have not been fractionated from each other during melting, then it is unlikely that CO₂ was fractionated from either. Fractionation of Ba and Nb will generate variations in the Ba/Nb ratio of melts with Ba and Nb concentration. Figure 4a shows this is not seen in any of the eruptions in this study, or the other Icelandic eruptions in the compilation. The scatter in Ba/Nb ratio arises largely from analytical imprecision, but could also reflect small scale source heterogeneity.

Another approach to assessing elemental fractionation during melting is to compare the variability of trace element concentrations. The more incompatibly an element behaves during melting, the

greater its variability amongst instantaneous fractional melts of the mantle. If two elements in a dataset have the same mean-normalised variance, the melting process has not fractionated the elements from each other (Rudge et al., 2013). The relative variance of Ba and Nb for each Icelandic melt inclusion suite are shown together in Figure 4b, providing further evidence that Ba and Nb have not been fractionated from each other. Elements more compatible than Nb have been fractionated from each other, as demonstrated by their relative variances (Supplementary Figure 3).

Assuming that the behaviour of CO₂ during mantle melting can be modelled as an incompatible element, and that it has a partition coefficient between that of Ba and Nb (Rosenthal et al., 2015), the apparent lack of fractionation between Ba and Nb would suggest that primary magmatic CO₂/Ba and CO₂/Nb ratios will record mantle source ratios.

3.3. Processes controlling CO₂-trace element systematics

Háleyjabunga and Stapafell both display correlations between CO₂ and Ba concentrations (Figure 2). Additionally, Háleyjabunga shows the increased variance of CO₂ concentration with Ba concentration that is typical of datasets generated by partial degassing and mixing (Matthews et al., 2017). Stapafell exhibits somewhat more complexity, possibly due to a more prolonged history of mixing and fractional crystallisation. Heilagsdalsfjall and Berserkjähraun do not exhibit correlations between CO₂ and Ba concentrations, likely a result of more extensive degassing and mixing.

Three Háleyjabunga melt inclusions (without bubble corrections) form a sub-population with higher CO₂ concentrations than the other Háleyjabunga melt inclusions (Figure 2). The higher CO₂ concentrations may reflect inclusion entrapment at an earlier stage of magma evolution, where the melts had higher CO₂ concentrations due to a greater storage pressure or by less mixing having taken place. The highest CO₂/Ba ratio in the Háleyjabunga melt inclusions also comes from within this sub-population; if the population is derived simply from being trapped earlier, then this is the value of CO₂/Ba most likely to reflect the Háleyjabunga mantle source. However, to fully assess this hypothesis by consideration of the sub-population's CO₂-trace element systematics requires a much larger sample size. Alternatively, these inclusions may reflect CO₂ being added to depleted melts,

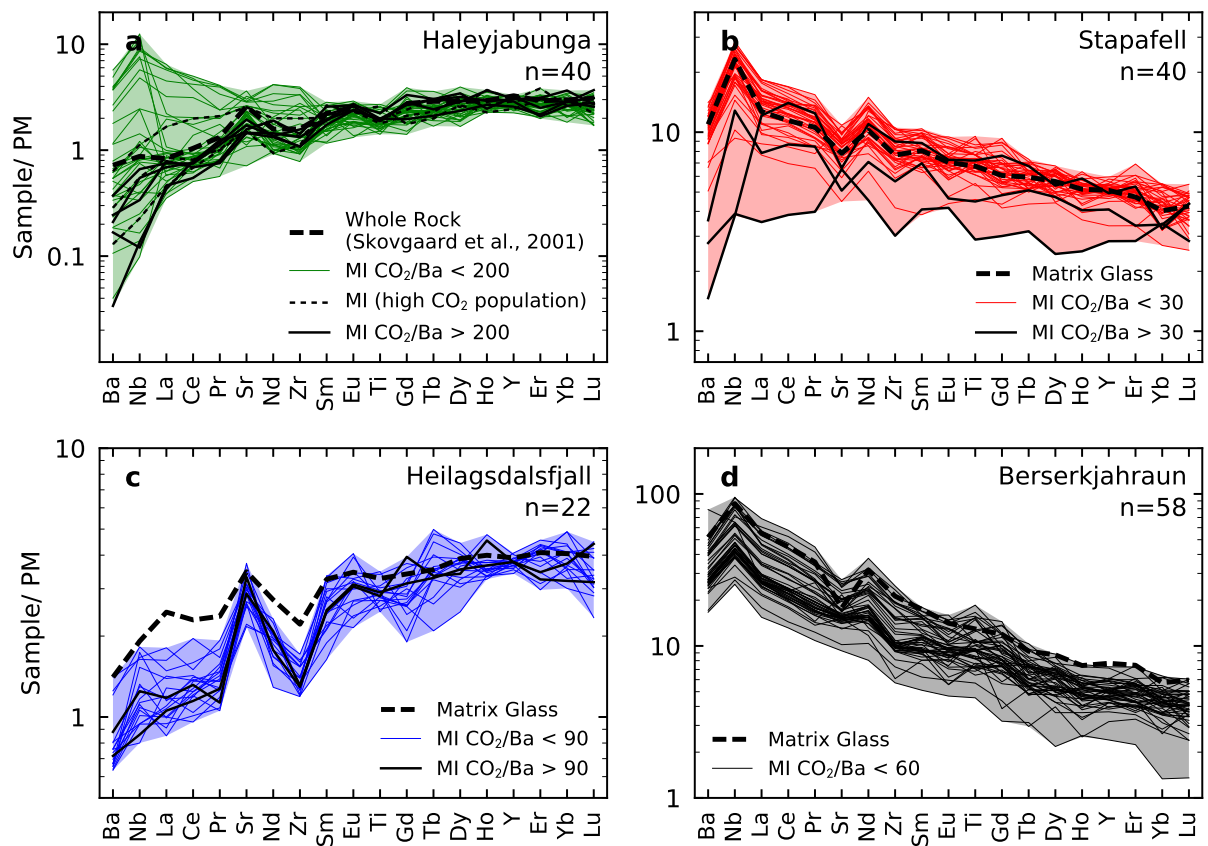


Figure 3: Normalised melt inclusion trace element concentrations. The region between the most extreme melt inclusions of each eruption is shown by shading. Also shown (as thick dashed lines) are the means of matrix glasses analyses for Stapafell, Heilagsdalsfjall and Berserkjahraun, and the whole rock analysis of Hálleyjabunga reported by Skovgaard et al. (2001). The melt inclusions preserving the highest CO_2/Ba ratios are highlighted in black, with the threshold CO_2/Ba used reported in the legend for each panel. All analyses are normalised to the primitive mantle of Palme and O'Neill (2003).

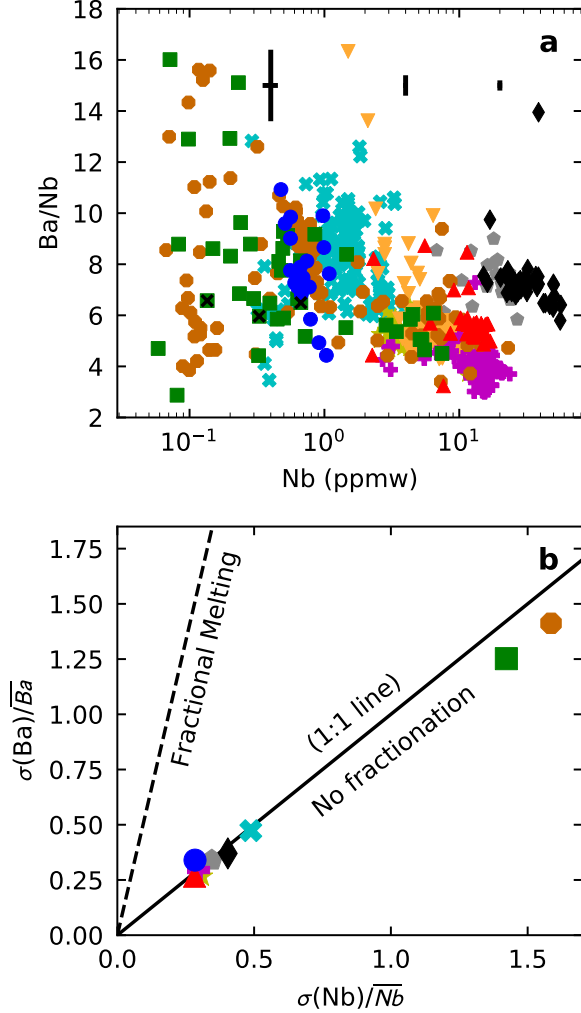


Figure 4: Panel a shows the Ba/Nb ratio of the melt inclusions from the eruptions in Figure 1. Three representative error bars are shown, illustrating the 1 s.d. precision on the Ba/Nb ratio and Nb concentrations with varying enrichment, calculated from variably enriched secondary standard analyses. The highest Ba/Nb values for Miðfell (Miller et al., 2019) fall off the top of the plot. Panel b compares the standard deviation of Ba and Nb in melt inclusions from each eruption, normalised to their mean. The solid line shows the expected relationship if the two elements are not fractionated from each other during melting, the dashed line shows the expected relationship if they are fractionated by perfect fractional melting (Rudge et al., 2013), using the partition coefficients from Workman and Hart (2005).

possibly by dissolution of CO₂ vapour or by melting in the presence of graphite. Both processes can elevate CO₂ concentrations and CO₂/Ba ratios of depleted melts, and are discussed further in Appendix B. Since we cannot be certain these inclusions represent mantle CO₂/Ba ratios, we choose to discount them from the following discussion.

4. Systematics of the Global Melt Inclusion Array

In Figure 5 we compare our new CO₂ and Ba data from Háleyjabunga, Stapafell, Heilagsdalsfjall and Berserkjahraun, with other Icelandic melt inclusion suites and those from ocean-island and mid-ocean ridge settings. We exclude inclusions from arc volcanoes since their enrichment in H₂O complicates our understanding of CO₂ solubility. In both the Iceland compilation (Figure 5a) and the global compilation (Figure 5b), there is a striking negative correlation between CO₂/Ba and Ba concentration. This correlation is bounded above and below by lines of constant CO₂ concentration, though bubble-corrected inclusions (unfilled symbols) break through this upper bound. For the most depleted inclusions the low bound corresponds to approximately 100 ppmw CO₂, and the high bound to 1000-1400 ppmw CO₂. The same systematic is observed in CO₂/Nb–Nb space (Supplementary Figure 4).

4.1. A global array reflecting mantle CO₂ heterogeneity?

The negative correlation between CO₂/Ba and Ba concentration could be caused by source heterogeneity. The trace-element enriched mantle reservoirs that contribute disproportionately to the Ba-enriched melts may not have corresponding CO₂ enrichments. However, as the negative correlation has the same position and gradient in both the Icelandic and global datasets, this would imply depleted and enriched mantle components occur with the same distinct CO₂/Ba and CO₂/Nb ratios everywhere. Radiogenic isotope constraints demonstrate that there is substantial variation in the chemistry of enriched and depleted components globally, even between highly incompatible elements that are difficult to fractionate during partial melting (e.g. U and Rb) (Stracke et al., 2005). It is therefore perhaps unlikely that these heterogeneous components would be characterised by single CO₂/Ba and CO₂/Nb ratios.

Furthermore, the presence of CO₂-rich shrinkage bubbles in many of these inclusions demonstrates that many of the melts must have contained more CO₂ in the past, which would have placed them originally above the global array. This is particularly apparent for melt inclusions from Berserkjahraun, Miðfell, Laki and Surtsey (Figure 5a).

4.2. A global array controlled by degassing?

A simpler explanation than source heterogeneity is the operation of a process limiting the CO₂ concentration within the melt inclusion. The most obvious process is degassing. In this case, the lower limit of CO₂ on the array corresponds to CO₂ solubility for magma storage in shallow crustal magma chambers. The small number of inclusions with lower CO₂ concentrations than this probably owe their undersaturation to degassing during eruption, or mixing with extremely CO₂-depleted partial mantle melts (Matthews et al., 2017). The upper bounds on CO₂ concentration in depleted melt inclusions of 1000–1400 ppmw correspond to saturation pressures in the range of 1–3 kbar, depending on the solubility model chosen (Figure 6, Supplementary Figures 5 and 6). This pressure range coincides with that expected for olivine decrepitation (Wanamaker et al., 1990; MacLennan, 2017), where the crystal undergoes brittle failure when it can no longer support the pressure difference between the inclusion and its surroundings. Experiments by Wanamaker et al. (1990) predict that overpressures of up to 2.2 kbar may be supported. This is very close to the maximum entrapment pressure of the moderately-depleted inclusions when calculated with the CO₂ solubility model of Iacono-Marziano et al. (2012), demonstrated in Figure 6.

Figure 5b demonstrates the presence of two different upper limits; one for more depleted eruptions and one for more enriched eruptions. If decrepitation is the process responsible for the upper limit of the array, the limits for both enriched and depleted eruptions ought to correspond to the CO₂ solubility at 2.2 kbar. However, the dependence of CO₂ solubility on melt composition allows significantly different CO₂ concentrations to equilibrate at the same pressure in different melts. Melt polymerisation tends to reduce CO₂ solubility, whilst the presence of cations with an affinity for forming carbonate complexes increases CO₂ solubility (Shishkina et al., 2014).

The enriched inclusions are significantly richer in total-alkalis (Na₂O + K₂O) for similar SiO₂ con-

tents (Supplementary Figure 7), but this does not translate into significant differences in the π^* compositional parameter used by Shishkina et al. (2014) in their CO₂ solubility model (Supplementary Figure 8). Though the concentration of alkali elements in the enriched inclusions acts to increase the CO₂ solubility, their lower MgO and CaO concentrations tends to decrease CO₂ solubility (Dixon, 1997). As the decrepitation limit should not vary strongly with eruption enrichment, it is likely that the higher CO₂ bound for the enriched melts is solubility related, even if not captured by π^* .

A compositional-solubility effect creating the different bounds to the global array is supported by recent experimental work by Allison et al. (2019). By performing new experiments at intermediate pressure and alkaline compositions, Allison et al. (2019) show that existing CO₂ solubility models provide inadequate predictions of CO₂ solubility in more alkaline melts. Though the least alkaline experimental melt composition used by Allison et al. (2019) is more alkaline than the majority of eruptions from which melt inclusions are displayed in Figure 5, their empirical expression for CO₂ solubility likely incorporates other compositional effects of importance for the more enriched eruptions considered here. Figure 6 demonstrates that applying the empirical expression to the more enriched eruptions brings their saturation pressures into line with the depleted eruptions, when the CO₂ solubility model by Iacono-Marziano et al. (2012) is applied to the inclusions from depleted eruptions. However, a discrepancy exists if the saturation pressures for depleted eruptions are calculated using the models by Shishkina et al. (2014) and Eguchi and Dasgupta (2018a) (Supplementary Figure 5).

5. Identifying mantle CO₂ heterogeneity

The gross structure of both the Icelandic and Global melt inclusion arrays shown in Figure 5 is primarily controlled by low-pressure processes: storage in shallow magma chambers and olivine decrepitation (Section 4). However, many eruptions sit almost entirely within the bounds imposed by shallow storage and decrepitation, or have partitioned a significant fraction of their CO₂ budget into bubbles and thereby overcoming the decrepitation threshold. Many of these datasets may still preserve the CO₂/Ba ratios of their melts at the time of entrapment.

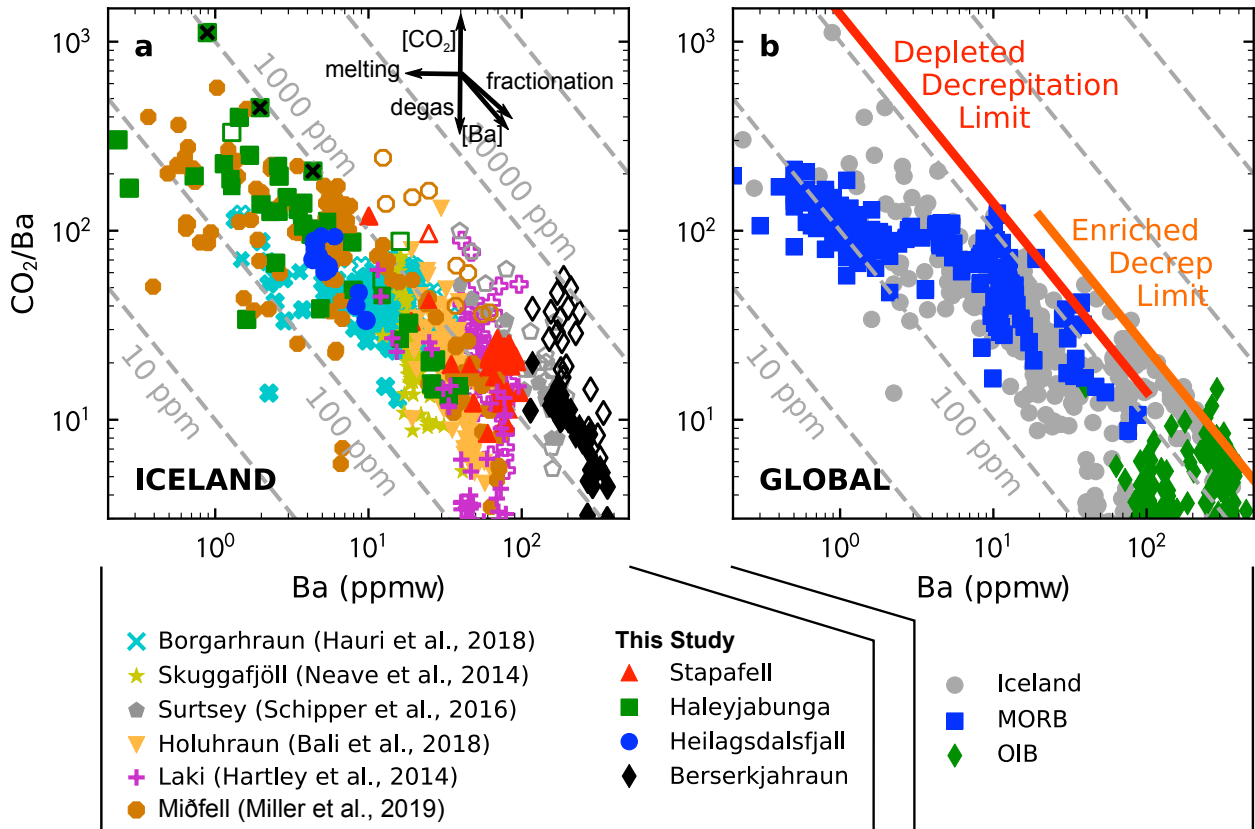


Figure 5: CO_2/Ba ratios in the melt inclusion glass for the four eruptions studied here, and compiled data from other eruptions in Iceland (panels a and b), from along the mid-ocean ridge system (MORB), and from ocean-islands (OIB) (panel b). Filled symbols show values for CO_2/Ba derived from CO_2 hosted in the glass only, open symbols show the values of CO_2/Ba where bubbles (measured by Raman) have been added back to the glass. The vectors in panel a show the effects of mantle melting, fractionation during melting, CO_2 degassing, CO_2 addition, and Ba addition. Diagonal dashed-grey lines show constant CO_2 concentration (10 ppm, 100 ppm, 1000 ppm, 1 wt%, and 10 wt%). Solid red and orange lines in panel b show the inferred decrepitation limits at 1400 ppmw and 2400 ppmw respectively. The 1 s.d. uncertainty is the size of the markers. Most OIB data falls off the bottom of the figure. Data from Hauri et al. (2018); Hartley et al. (2014); Neave et al. (2014); Schipper et al. (2016); Bali et al. (2018); Le Voyer et al. (2017); Saal et al. (2002); Sides et al. (2014); Wanless and Shaw (2012); Wanless et al. (2014); Cabral et al. (2014); Métrich et al. (2014); Wanless et al. (2015); Tucker et al. (2019).

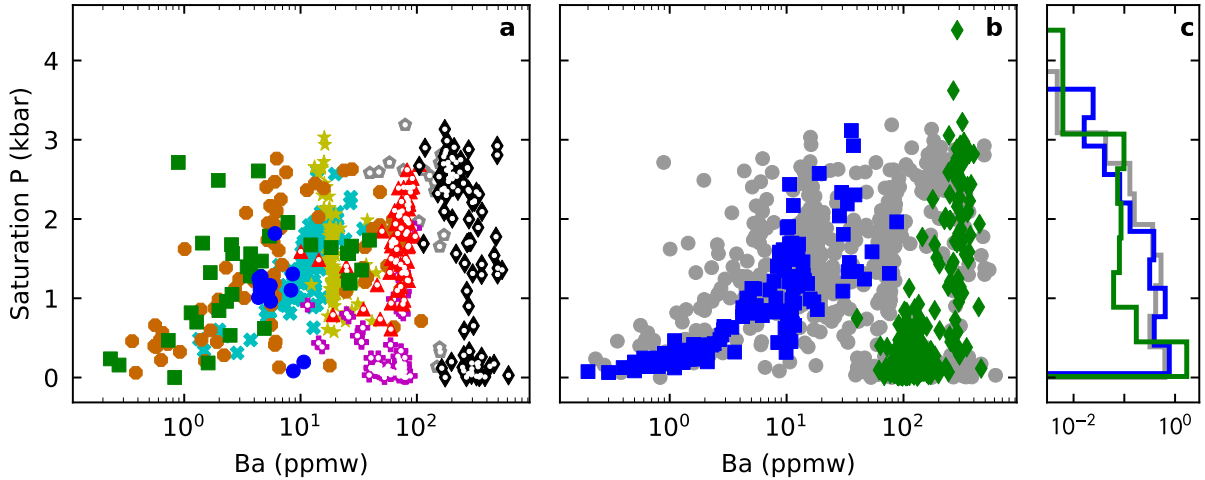


Figure 6: The pressure of CO_2 vapour saturation for each melt inclusion in the Iceland compilation (panel a), and the global compilation (panels b and c). Symbols as used in Figure 5. Saturation pressures for melt inclusions from depleted Icelandic eruptions and MORB are calculated using the CO_2 solubility model by Iacono-Marziano et al. (2012). Saturation pressures for melt inclusions from enriched Icelandic eruptions (symbols overlaid by white dots in panel a) and OIB are calculated using the power-law fit to experimental data for ‘Sunset Crater’ by Allison et al. (2019). The effect of H_2O is neglected in all calculations, as the melts contain sufficiently low H_2O concentrations that CO_2 solubility will be little affected. The calculations do not include bubble-corrections.

However, all the melt inclusion datasets considered here show significant internal variability in the CO_2/Ba ratios they preserve. Matthews et al. (2017) argued that the diversity of CO_2/Ba ratios within eruptions indicates that they have experienced partial CO_2 loss by degassing, but can regain a positive (albeit scattered) correlation between CO_2 and Ba by magma mixing. We consider the implications of concurrent degassing and mixing for identifying mantle CO_2/Ba in Section 5.1. Another plausible explanation for diversity in CO_2/Ba ratios is the mapping of source CO_2/Ba heterogeneity into its melts. In Section 5.3 we argue such small heterogeneities are likely to be homogenised for individual eruptions during melt generation and transport. Applying the methodology developed in Sections 5.1 and 5.3 to the melt inclusion compilation from Iceland, supplemented with our new data, we identify and place quantitative constraints on CO_2 heterogeneity within the Icelandic mantle plume (Section 5.4). We then explore in Section 5.7 whether this approach yields information on the global variability of CO_2 in the upper mantle, as sampled by mid-ocean ridge basalts (MORBs).

5.1. Has concurrent degassing and mixing removed the mantle CO_2/Ba signal?

A consequence of concurrent degassing and magma mixing is that the average value of CO_2/Ba for an eruption is more sensitive to the degassing pressure than to the CO_2/Ba ratio inherited by the primary melts from their mantle source. Since the degassing, mixing and decrepitation processes all act to lower the CO_2/Ba ratio recorded by melt inclusions, it follows that the maximum CO_2/Ba value observed in melt inclusions from a single eruption is the value least affected by CO_2 loss and therefore most likely to preserve the mantle CO_2/Ba ratio.

Any given melt inclusion dataset samples a population of melts with CO_2/Ba ratios ranging from very low up towards the mantle value. The likelihood of the dataset to sample the true maximum CO_2/Ba ratio (the mantle value) depends on the relative proportions of these melts, described statistically by a probability distribution. An eruption’s CO_2/Ba distribution may have a long low-probability tail towards the mantle value, depending on the extent of degassing prior to mixing and the efficiency of mixing. Without knowledge of the distribution of melts entering the crust, and the history of degassing and mixing they subsequently un-

dergo, it is impossible to constrain the shape of this distribution and therefore assess the likelihood of a given melt inclusion suite preserving the mantle CO_2/Ba ratio in one or more of the inclusions.

Though we cannot tell whether an individual dataset preserves the mantle CO_2/Ba ratio when taken in isolation, comparison with a large number of melt inclusions from a diversity of eruptions can provide a context in which to consider the maximum CO_2/Ba values preserved by an individual eruption. If the maximum CO_2/Ba ratios of eruptions vary systematically with their mantle sources, and systematic biases from crustal processing can be ruled out, then greater confidence may be placed in the recorded CO_2/Ba ratios reflecting their mantle source.

5.2. Are high CO_2/Ba and CO_2/Nb ratios analytical artefacts?

To avoid interpreting analytical artefacts, Rosenthal et al. (2015) and Hirschmann (2018) avoid using the highest CO_2/Ba values, suggesting these analyses may have incorporated carbon derived from cracks in the sample. Standard practice when collecting melt inclusion datasets is to avoid analyses in the vicinity of cracks, and the ^{12}C count rates would vary erratically in such a situation. In carefully collected datasets such analytical artefacts will be eliminated, and it is more likely that the highest CO_2/Ba ratios instead reflect sampling of low probability-density tail to the CO_2/Ba distribution. Furthermore, the inclusions with the highest CO_2/Ba and CO_2/Nb have CO_2 concentrations that are within the range of the rest of the dataset, and not anomalously high as might be expected if it were an analytical artefact.

In Supplementary Figures 9 and 10 we demonstrate the difference between taking the dataset maximum CO_2/Ba and CO_2/Nb ratios, as opposed to the upper limit of the main CO_2/Ba and CO_2/Nb data density. The dataset maximum CO_2/Ba ratios do not coincide with extreme values of Ba/Nb (Supplementary Figure 11) or anomalous trace element chemistry (Supplementary Figure 12), suggesting the high values are also not derived from analytical artefacts in trace element concentration measurements. The lack of coincidence between high CO_2/Ba and extreme Ba/Nb provides further evidence that the highest CO_2/Ba ratios do not arise from fractionation between Ba , Nb and CO_2 during melting.

5.3. Preservation of small-scale mantle CO_2 heterogeneity in melts

In applying the method described above, we are implicitly assuming that the CO_2/Ba ratio of a single melt inclusion is representative of the heterogeneous mantle that contributes melt to the whole eruption. However, mantle-derived Pb-isotope heterogeneity is present within melt inclusions from single Icelandic eruptions, including single hand-specimens from Háleyjabunga and Stapafell (MacLennan, 2008b). This observation clearly demonstrates that heterogeneity in Pb-isotope ratios survives the melting and melt transport processes operating beneath Iceland.

However, CO_2 , Ba and Nb are much more incompatible than Pb and are likely to be almost entirely removed from the solid residue in the first increments of melting. Though channelised mantle flow can transport significant mantle derived chemical heterogeneity in melts, the deepest melts are likely to be well mixed (Spiegelman and Kelemen, 2003; Kelemen et al., 1997), and may subsequently be diluted in varying amounts by higher degree melts. We therefore consider it likely that single eruptions will have mixed out any heterogeneity in CO_2/Ba and CO_2/Nb ratios that was present within their mantle source regions. If this is correct, we must look for carbon heterogeneity on an eruption to eruption basis rather than within single eruptions.

By taking the maximum CO_2/Ba ratio of a melt inclusion dataset we are assuming this is representative of the average mantle sampled by the eruption, as argued above. When we make the comparison between this CO_2/Ba value, and the bulk-rock radiogenic isotope ratios, we must assume that the isotope ratios are representative of the same mantle average. Since Pb , Sr , and Nd are more compatible than CO_2 and Ba , melts containing these elements are generated at higher melt fractions, and source heterogeneity can survive melting and transport (Spiegelman and Kelemen, 2003; Kelemen et al., 1997). If the whole rock lava from which the radiogenic isotope measurements are made does not reflect complete mixing of these diverse melts, the Pb -, Sr -, and Nd -isotope ratios may be decoupled from the maximum CO_2/Ba and CO_2/Nb seen in melt inclusions.

Additionally, higher extents of melting are required for a mantle component to contribute to the Nd , Sr , and Pb budget of a magma, than for it to contribute to the CO_2 , Ba , and Nb budget. Where

the extent of melting is controlling the relative contribution of depleted and enriched mantle to the Pb-, Nd-, and Sr-isotope ratios, rather than source composition, the radiogenic isotopes and the maximum CO₂/Ba and CO₂/Nb in melt inclusions may reflect averages of different proportions of the enriched and depleted components in the source.

For the influence of these processes to be properly assessed a much larger number of plausibly undegassed melt inclusion datasets is required. We, therefore, do not consider the possibility of CO₂/Ba and radiogenic isotope decoupling further. A more robust comparison could be made with radiogenic isotopes of an element at least as incompatible as Nb. One such system is ³He/⁴He which we use in complement to Pb-, Nd- and Sr-isotopes in the following analysis.

5.4. Heterogeneity within the Icelandic plume

Radiogenic isotope observations require multiple enriched and depleted source components within the Icelandic mantle (Thirlwall et al., 2004; Peate et al., 2010; Shorttle et al., 2013). We will use our new data to evaluate whether these mantle components also differ in their CO₂ content. The Pb-, Nd-, and Sr-isotope systems are sensitive to ancient melt extraction and recycling events, whilst the ³He/⁴He system is diagnostic of primordial (or undegassed) mantle reservoirs.

Though there is a large quantity of melt inclusion data from Iceland, from a number of spatially and temporally restricted eruptions with diverse geochemistry, it is not yet sufficient to fully resolve the CO₂ concentrations in the diversity of mantle components beneath Iceland. We therefore proceed on the basis of finding the minimum number of distinct components required to explain the coupled CO₂/Ba and radiogenic isotope observations, whilst acknowledging the end-members we invert for are some average of the full diversity of heterogeneities present in the Icelandic mantle.

Figures 7a and 7b demonstrate there is no systematic covariation of CO₂/Ba within ²⁰⁶Pb/²⁰⁴Pb–²⁰⁸Pb/²⁰⁴Pb space, nor ⁸⁷Sr/⁸⁶Sr–¹⁴³Nd/¹⁴⁴Nd space. Though not shown here, this is also true of any combination of Pb-isotopes with Sr- and Nd-isotopes. Whilst the lithophile isotope systems excel at separating contributions from enriched and depleted mantle reservoirs, the primordial mantle lies in the middle of lithophile isotope space (Hart et al., 1992). Helium isotopes, in contrast, reveal contributions from primordial man-

tle components clearly, as primitive mantle has extremely high ³He/⁴He ratios (e.g., Class and Goldstein, 2005).

When ³He/⁴He ratios are plotted with ¹⁴³Nd/¹⁴⁴Nd ratios (Figure 7c) a covariation of CO₂/Ba with position across the space does emerge: mantle material with high (primordial) ³He/⁴He is associated with high magmatic values of CO₂/Ba, whilst melts derived from depleted mantle (with $R/R_a \sim 8$) have moderate CO₂/Ba and those from enriched mantle (with $R/R_a \leq 8$) have low CO₂/Ba. The same trends are observed if CO₂/Nb is used in place of CO₂/Ba (Supplementary Figure 13), and a similar co-variation is observed if the upper-limits of the CO₂/Ba and CO₂/Nb ratios in the main data population are used in place of the dataset maxima (Supplementary Figures 14 and 15).

The association of high CO₂/Ba with primordial undegassed mantle material was first made by Miller et al. (2019), based on the elevated CO₂/Ba ratios seen in the Miðfell eruption in Iceland. By making a comparison to melt inclusions from Borgarhraun (Hauri et al., 2018), Miller et al. (2019) argue that the elevation in CO₂/Ba in Miðfell is not caused by crustal processing, since both eruptions have similar trace element concentrations. Though it could be argued that Borgarhraun has seen more extensive CO₂ loss by magmatic degassing prior to inclusion entrapment, this seems unlikely given the high (6–8 kbar) pressures of crystallisation (Winpenny and MacLennan, 2011; Neave and Putirka, 2017) and the Borgarhraun melt inclusions’ distance from the decrepitation threshold (Figure 5a). Our new data from Háleyjabunga lends further support to hypothesis of Miller et al. (2019) that primordial mantle domains are associated with high CO₂/Ba.

However, the same argument cannot be used when making a comparison to the more enriched eruptions, such as Berserkjahraun and Stapafell, as they have significantly higher trace element concentrations in their melt inclusions. If these melts started off with the same or higher CO₂/Ba ratio than Borgarhraun, the Stapafell and Berserkjahraun melts should have considerably higher CO₂ concentrations. Such high CO₂ concentrations make these melts more susceptible to degassing and the inclusions more susceptible to CO₂ gas loss during decrepitation; crustal processing will therefore tend to introduce a systematic bias towards low CO₂/Ba ratios in enriched magmas. Regardless of

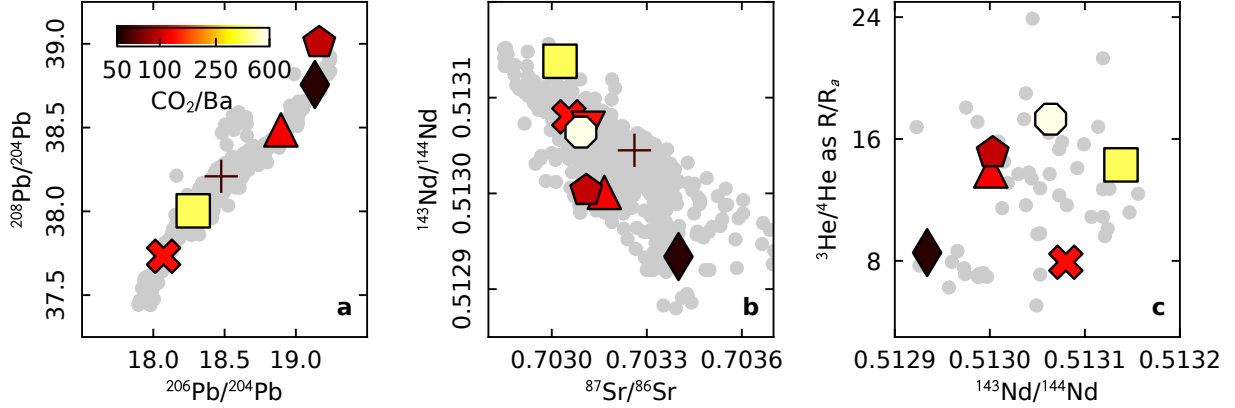


Figure 7: Radiogenic isotope compositions of the whole rocks from eruptions discussed in this text (large symbols), data sources are given in Supplementary Table 3. The symbols used are the same as in Figure 5, but each symbol is colored for the maximum CO_2/Ba ratio observed in melt inclusions from that eruption, as described in the text. Grey circles show the compilation of Iceland whole-rock isotope analyses, data sources are given in the Supplementary Information.

whether the low CO_2/Ba in the enriched Berserkjahraun magmas is a result of low CO_2/Ba in the enriched source or not, we require at least three end-members to deconvolve the primordial mantle signal.

5.4.1. Inverting for mantle endmember CO_2 concentrations

Here we consider mixing between three mantle end-members:

1. *Depleted mantle (DM)*- containing low trace element concentrations with radiogenic Nd- and He-isotope ratios ($R/R_a \sim 8$), typical of the MORB-source mantle
2. *Enriched mantle (EM)*- containing higher trace element concentrations with unradiogenic Nd-isotopes and radiogenic He-isotope ratios ($R/R_a \leq 8$), representing recycled material
3. *Primordial mantle (PM)*- containing trace element concentrations and isotope ratios typical of bulk silicate Earth.

The numerical values of their geochemical properties are given in Table 1.

In principle, a mixing surface which closely matches the covariation of CO_2/Ba across $^{143}\text{Nd}/^{144}\text{Nd}$ - $^3\text{He}/^4\text{He}$ space can be found. Sohn (2013) developed a mathematical formulation for n-dimensional mixing hyperbolae, when mixing between three end-members this reduces to a surface in three-dimensions. Sohn (2013) demonstrated

that the 3-dimensional mixing problem can be reduced to 13 parameters, where Equation 1 is satisfied for values of CO_2/Ba , $^{143}\text{Nd}/^{144}\text{Nd}$ and $^3\text{He}/^4\text{He}$ lying on the mixing surface:

$$\det \mathbf{M} = 0 \quad (1)$$

where

$$\mathbf{M} = \begin{bmatrix} \left(\frac{\text{CO}_2}{\text{Ba}} - \left[\frac{\text{CO}_2}{\text{Ba}} \right]_{\text{DM}} \right) & \left(\frac{^{143}\text{Nd}}{^{144}\text{Nd}} - \left[\frac{^{143}\text{Nd}}{^{144}\text{Nd}} \right]_{\text{DM}} \right) \\ \left(\frac{\text{CO}_2}{\text{Ba}} - \left[\frac{\text{CO}_2}{\text{Ba}} \right]_{\text{PM}} \right) & K_1 \left(\frac{^{143}\text{Nd}}{^{144}\text{Nd}} - \left[\frac{^{143}\text{Nd}}{^{144}\text{Nd}} \right]_{\text{PM}} \right) \\ \left(\frac{\text{CO}_2}{\text{Ba}} - \left[\frac{\text{CO}_2}{\text{Ba}} \right]_{\text{EM}} \right) & K_3 \left(\frac{^{143}\text{Nd}}{^{144}\text{Nd}} - \left[\frac{^{143}\text{Nd}}{^{144}\text{Nd}} \right]_{\text{EM}} \right) \\ & \left(\frac{^3\text{He}}{^4\text{He}} - \left[\frac{^3\text{He}}{^4\text{He}} \right]_{\text{DM}} \right) \\ & K_2 \left(\frac{^3\text{He}}{^4\text{He}} - \left[\frac{^3\text{He}}{^4\text{He}} \right]_{\text{PM}} \right) \\ & K_4 \left(\frac{^3\text{He}}{^4\text{He}} - \left[\frac{^3\text{He}}{^4\text{He}} \right]_{\text{EM}} \right) \end{bmatrix} \quad (2)$$

The subscripts ‘DM,’ ‘PM,’ and ‘EM’ represent endmember values for the depleted, primordial and enriched components respectively. The parameters K_1 , K_2 , K_3 and K_4 represent ratios of source trace element concentration ratios:

$$K_1 = \frac{[\text{Nd}]_{\text{PM}}/[\text{Ba}]_{\text{PM}}}{[\text{Nd}]_{\text{DM}}/[\text{Ba}]_{\text{DM}}} \quad (3)$$

$$K_2 = \frac{[\text{He}]_{\text{PM}}/[\text{Ba}]_{\text{PM}}}{[\text{He}]_{\text{DM}}/[\text{Ba}]_{\text{DM}}} \quad (4)$$

$$K_3 = \frac{[\text{Nd}]_{\text{EM}}/[\text{Ba}]_{\text{EM}}}{[\text{Nd}]_{\text{DM}}/[\text{Ba}]_{\text{DM}}} \quad (5)$$

$$K_4 = \frac{[\text{He}]_{\text{EM}}/[\text{Ba}]_{\text{EM}}}{[\text{He}]_{\text{DM}}/[\text{Ba}]_{\text{DM}}} \quad (6)$$

i.e., source trace element concentrations will trade off against each other to yield identical surfaces. By combining the concentration ratios into four parameters, the number of free parameters in the inversion is reduced (Sohn, 2013).

In order for our prior assumptions about mantle source chemistry to be applied consistently, we take a Bayesian approach to estimating the CO_2/Ba ratio and CO_2 concentration of the mantle sources. The prior distributions for end-member properties are described in Table 1 and its caption. For the K_n parameters log-uniform distributions from 10^{-6} to 10^6 were used. We implement the Bayesian calculation using the importance nested sampling Monte-Carlo inversion routine ‘Multinest’ (Feroz and Hobson, 2008; Feroz et al., 2009, 2013) with the pymultinest python wrapper (Buchner et al., 2014). For simplicity we ignore the uncertainty in the $^{143}\text{Nd}/^{144}\text{Nd}$ and $^3\text{He}/^4\text{He}$ ratios of the samples, calculating the log-likelihood of each mixing model based only on the misfit between the CO_2/Ba of the eruption and modelled mixing surface. The total log-likelihood is calculated by summing contributions from each eruption:

$$\ln(L) = \sum_1^n \ln(L_n(\mu_n, \sigma_n, x_n)) \quad (7)$$

where μ_n is the observed CO_2/Ba ratio, and σ_n is its one standard deviation uncertainty. The value of CO_2/Ba ratio on the modelled mixing surface (x_n) is calculated by numerically solving Equation 1, given the observed $^{143}\text{Nd}/^{144}\text{Nd}$ and $^3\text{He}/^4\text{He}$ ratios of the samples.

Since the Beserkjahraun, Stapafell, and Surtsey melt inclusions have maximum CO_2/Ba ratios that fall close to the decrepitation threshold (Figure 5), we treat these observations as minimum bounds on the CO_2/Ba mixing surface. Models which place the mixing surface at lower values of CO_2/Ba ratio are penalised by an exponential contribution to the log-likelihood:

$$\ln(L_n) = \begin{cases} -\exp\left((\mu_n - x_n)^2\right), & \text{if } \mu_n < x_n \\ 0, & \text{otherwise} \end{cases} \quad (8)$$

Haleyjabunga, Miðfell and Borgarhraun preserve inclusions with high CO_2/Ba ratios considerably below the decrepitation threshold; therefore, they

provide the most direct constraint on the mixing surface. Their contribution to the log-likelihood function reflects their squared normalised distance from the surface:

$$\ln(L_n) = -\frac{(x_n - \mu_n)^2}{\sigma_n^2} \quad (9)$$

This expression is equivalent to the expression for log-likelihood assuming the constraints follow a normal distribution, with the constant terms removed (Lee, 2012).

Inverting the Sohn (2013) mixing equations provides estimates for only CO_2/Ba ratios of the three end-members, and not their CO_2 concentrations. To estimate CO_2 concentration we employ a Monte-Carlo calculation pairing values drawn from the posterior CO_2/Ba distributions of each end-member with a randomly selected value from a prior distribution of Ba concentrations of each mantle source (Table 1).

5.4.2. Inversion results

The results of the inversion are shown in Figure 8 and Table 2, they represent the first CO_2 concentration estimates to be made for different mantle components in one location. Figure 9 shows that our estimate for the depleted mantle CO_2 concentration (102_{-14}^{+21} ppmw) compares favourably with the concentrations inferred from MORB melt inclusion suites (Rosenthal et al., 2015; Le Voyer et al., 2017), undersaturated glasses (Michael and Graham, 2015) and with estimates derived from CO_2 -He systematics (Marty, 2012; Tucker et al., 2018). Our new estimate for primordial mantle ($2.15_{-1.49}^{+0.94}$ wt%) is much higher than previous estimates of the CO_2 content of plume mantle, or bulk mantle as estimated by Marty (2012), whilst our estimate of CO_2 concentration in the recycled mantle (68_{-64}^{+1170} ppmw) is significantly lower than the plume and bulk mantle estimates. This difference most likely arises from previous estimates averaging high- and low- CO_2 mantle reservoirs.

The Depleted Mantle

When the DM CO_2/Ba prior is left open, the inversion routine finds two likelihood maxima; one solution places the high mantle CO_2 concentrations into the DM-endmember rather than the PM-endmember. Since previous work has shown the depleted mantle has moderately low CO_2 concentrations (e.g., Saal et al., 2002; Hirschmann, 2018;

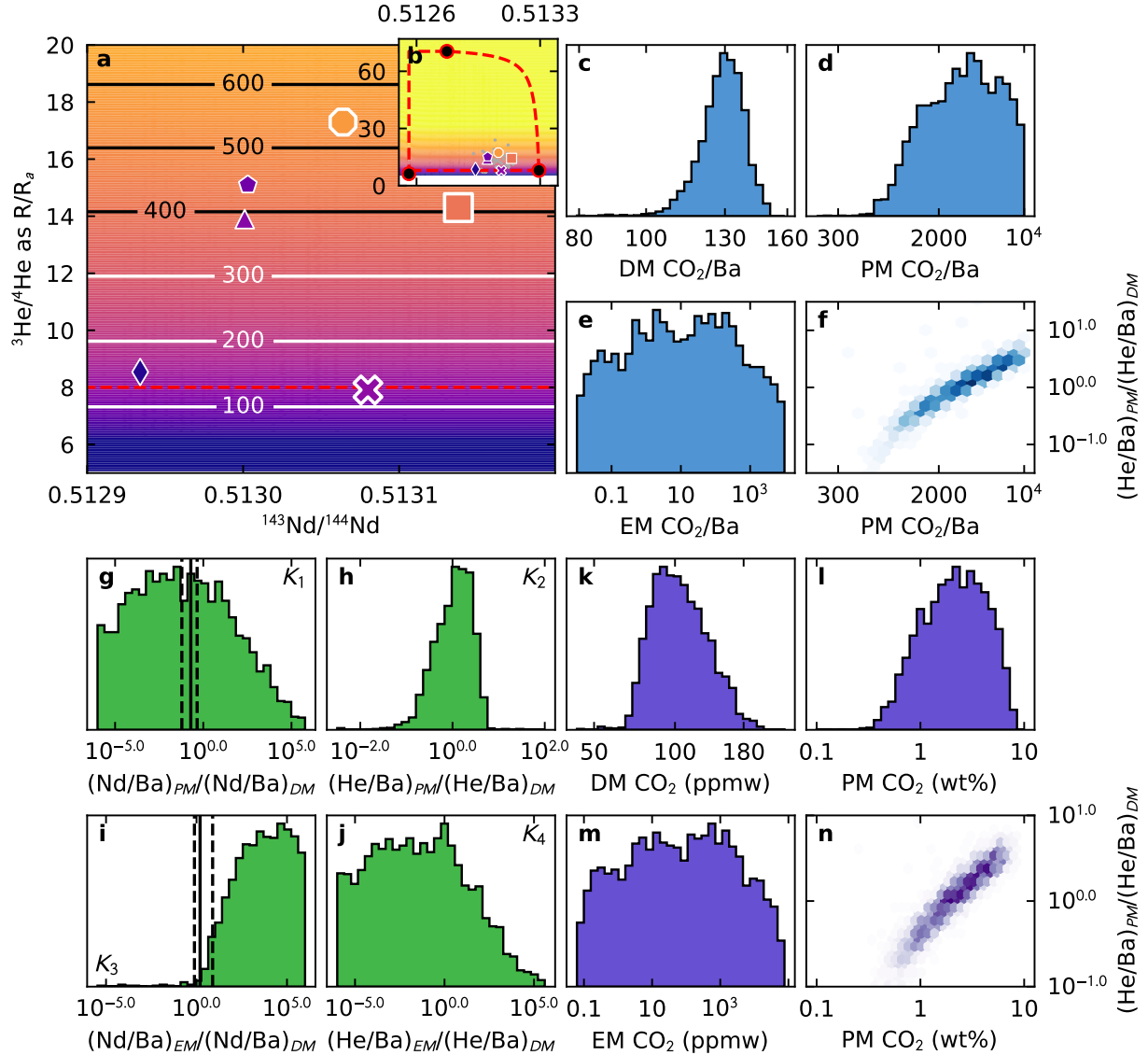


Figure 8: Results of the Bayesian inversion for mantle endmember CO₂ concentrations, assuming Haleyjabunga, Miðfell, and Borgarhraun (large symbols in panel a) preserve mantle CO₂/Ba ratios, whilst Berserkjahraun, Stapafell, and Surtsey (small symbols in panel a) provide only minimum bounds. The colour shading in panels a and b represents the CO₂/Ba ratio of the fitted surface, with the scale saturating below 50 and above 1200. The eruptions are coloured for their CO₂/Ba observations on the same scale. The black contours on panel a also show CO₂/Ba ratio. The dashed red lines on panels a and b show the extreme mixing boundaries. Panels c–e show the posterior distributions for end-member CO₂/Ba. Panel f shows the trade-off between PM CO₂/Ba and K_2 as a 2D histogram with shading indicating data density. Panels g–j show the posterior distributions for K_1 – K_4 . The vertical lines in panels g and i show the values for the solid mantle calculated using Nd and Ba estimates from Workman and Hart (2005) and Stracke et al. (2003). Panels k–m show the posterior CO₂ concentrations calculated from the posterior CO₂/Ba distributions. Panel n shows the trade-off between mantle CO₂ concentration and K_2 .

Parameter	DM	EM	PM
CO ₂ /Ba	50–150 ^a	0.01 – 1 × 10 ⁴	1 – 1 × 10 ⁴
(log-uniform)	See caption ^a	Upper limit ~10 wt% CO ₂ in mantle	
¹⁴³ Nd/ ¹⁴⁴ Nd	0.5132–0.5134	0.5122–0.5129	0.512638–0.51290
	Su (2003)	See caption ^b	See caption ^c
R/R _a	8.00±0.05	5.0–7.4	50–95
	Kurz and Jenkins (1981)	See caption ^d	See caption ^e
Ba (ppmw)	0.58±0.32	2.55 ± 0.25	6.9 ± 1.0
	Workman and Hart (2005)	Stracke et al. (2003) ^f	Palme and O’Neill (2003)

Table 1: The priors set on the parameters in the inversions reported in the main text. The sources from which the priors are based are shown in the table. Where ranges are quoted for isotope ratios a uniform (or log-uniform) distribution between those bounds is used, for trace element concentrations it is a log-uniform distribution. Otherwise a normal distribution with the quoted mean and standard deviation are used. ^a the prior was chosen in order to obtain the solution where DM has moderate CO₂ concentrations, as inferred from previous studies. ^b The lower bound is lower than the most extreme basalts (e.g. Stracke et al., 2005), and the upper bound is just lower than the lowest Icelandic basalt. ^c The low Nd-isotope ratio bound for enriched mantle end-member is taken to be lower than the least radiogenic ocean island basalt (Stracke et al., 2005), and the high bound is taken to be lower than the least radiogenic observation from Iceland (Figure 1). ^d Lower bound is the R/R_a inferred for the EM2 mantle component by Jackson et al. (2007), and the upper bound is the ingrown R/R_a of the enriched component after 1 Ga. ^e Lower bound is the highest R/R_a observed in basalts derived from the Iceland plume (Stuart et al., 2003). The upper bound is the R/R_a predicted for entirely undegassed BSE-like mantle (Class and Goldstein, 2005). ^f Following Shorttle and MacLennan (2011), the trace element concentrations are taken as a third recycled crust (Stracke et al., 2003), and two thirds depleted mantle (Workman and Hart, 2005).

Endmember	CO ₂ /Ba	CO ₂ (ppmw)
DM	130 ⁺¹⁴ ₋₁₇	102 ⁺⁵³ ₋₂₇
EM	10 ⁺³⁴³⁰ ₋₁₀	67 ⁺²²⁰⁰⁰ ₋₆₇
PM	3190 ⁺⁵³⁷⁰ ₋₂₂₃₀	22000 ⁺³⁸⁰⁰⁰ ₋₁₅₀₀₀

Table 2: Summary of the inversion results described in the main text. Median values and the 5% and 95% confidence intervals are given for the CO₂/Ba, CO₂/Nb and CO₂ concentration of each of the three mantle endmembers (DM, EM and PM).

Hauri et al., 2018), and the primordial component has high CO₂ concentrations (Miller et al., 2019), we choose the DM CO₂/Ba prior such that only the likelihood-maxima corresponding to this low DM CO₂ solution is found (Table 1).

The Enriched Mantle

A consequence of treating the most enriched eruptions as minimum bounds in the inversion is the EM endmember becomes poorly constrained, and may have a CO₂/Ba ratio both lower or far in excess of the depleted mantle. Though the median EM CO₂/Ba ratio (~10) is significantly lower than for the DM endmember (~130), the posterior EM CO₂/Ba distribution depends strongly on the lower bound on the CO₂/Ba prior. The posterior distribution of K_3 (Figure 8i) is shifted to higher values than that expected from the Nd/Ba ratios of the DM and EM endmembers, shown by the verti-

cal lines (Workman and Hart, 2005; Stracke et al., 2003). This offset in K_3 most likely reflects fractionation during melting. The calculated CO₂/Ba ratio of the DM end-member is comparable to previous estimates for the upper mantle (Rosenthal et al., 2015; Hirschmann, 2018).

The Primordial Mantle

The calculated CO₂/Ba ratio of the PM end-member is extremely high. However, CO₂/Ba strongly trades-off against K_2 (the ratio of He/Ba ratios of PM and DM), this reflects the control of the K parameters on the shape of the surface and the distance of the PM end-member from the constraints. No significant trade-off is seen between PM CO₂/Ba ratio and the PM ³He/⁴He and ¹⁴³Nd/¹⁴⁴Nd ratios within the range of their priors.

Two alternative inversions were also performed. One where we do not assume Berserkjähraun, Stapafell and Surtsey are degassed and instead assume they also preserve mantle CO₂/Ba ratios (Supplementary Figure 16). In the second inversion we take the most extreme values of CO₂/Ba ratio observed in Haleyjabunga (Section 3.3) as the mantle source value (Supplementary Figure 17). The resulting surfaces are contorted and do not replicate the observations satisfactorily.

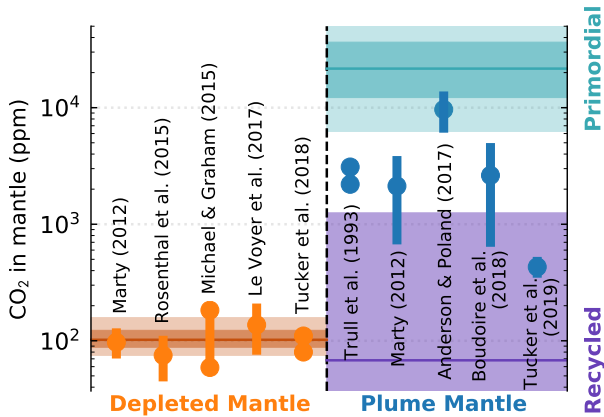


Figure 9: Comparison of our inversion results with previous estimates of the CO_2 concentration in depleted mantle and plume mantle. The horizontal bar shows the median value from the posterior distributions of CO_2 concentration, the dark shaded region shows the 25% and 75% confidence interval, and the light shaded region shows the 5% and 95% confidence interval (omitted for EM). The 25% percentile on the Recycled (EM) result plots below the lower limit of the y-axis. Published estimates from Marty (2012); Rosenthal et al. (2015); Michael and Graham (2015); Le Voyer et al. (2017); Tucker et al. (2018); Trull et al. (1993); Anderson and Poland (2017); Boudoire et al. (2018); Tucker et al. (2019)

5.5. Difficulties in inferring the recycled mantle CO_2 budget

We have demonstrated that reasonable constraints can be placed on the CO_2 budget of depleted and primordial mantle reservoirs. Difficulties remain, however, for identifying the CO_2 content of recycled mantle material. The first of these difficulties is made clear by the quantitative analysis above: eruptions which sample predominantly recycled mantle components are also extremely trace element enriched. If the CO_2/Ba of the recycled mantle material is similar or greater than the depleted mantle, the high trace element concentrations in enriched basalts results in a greater likelihood of CO_2 loss due to degassing and decrepitation.

A further difficulty is the possibility for decoupling between the extremely incompatible elements CO_2 , Ba and Nb, and the moderately incompatible elements Pb, Nd and Sr. As discussed in Section 5.3, this is unlikely to be an issue for the signal of high CO_2/Ba with high $^3\text{He}/^4\text{He}$, as He also behaves extremely incompatibly during mantle melting (Heber et al., 2007).

5.6. Implications of carbon rich mantle reservoirs

The extremely high CO_2/Ba ratio inferred for the primordial mantle in our inversion (Section 5.4) stems from the observations of high CO_2/Ba in melt inclusions from two eruptions. One way of rationalising this observation is if the primordial material is extremely depleted in lithophile trace elements, including Ba. Whilst it has been suggested that the high $^3\text{He}/^4\text{He}$ mantle may be more depleted than bulk silicate Earth (Hart et al., 1992), if the high $^3\text{He}/^4\text{He}$ mantle were to have similar CO_2 concentrations to the depleted mantle it must be at least an order of magnitude more depleted than the depleted mantle to explain the high observed CO_2/Ba ratio. Though our estimate for the primordial mantle CO_2 concentration ($2.15^{+0.94}_{-1.49}$ wt%) is higher than most previous mantle CO_2 estimates, it is considerably lower than the carbon content of CI and CM chondrites and similar to the carbon content of the enstatite chondrites, the likely building blocks of the Earth (Wasson and Kallemeyn, 1988).

Our estimate for the primordial mantle CO_2 concentration is primarily constrained by the inclusions from Háleyjabunga and Miðfell. These inclusions have slightly lower CO_2 concentrations (~ 500 ppmw), than inclusions from Borgarhraun (~ 1000 ppmw), the eruption constraining the depleted mantle CO_2 concentration. Magmas produced from a mantle source as rich in carbon as inferred for the primordial component might be expected to also be extremely CO_2 rich. However, in our model the Háleyjabunga and Miðfell inclusions have only a small contribution from the primordial component (Figure 8) causing their CO_2 concentrations to become substantially diluted, and allowing them to retain their mantle CO_2/Ba signal. The low trace element concentrations in Háleyjabunga and Miðfell are further evidence of substantial dilution by extremely trace element depleted melts.

This extremely high primordial mantle CO_2 budget is considerably greater than can be stored in the peridotite mineral assemblage (Rosenthal et al., 2015), though storage in silicate minerals is implicitly assumed when we treat CO_2 as a trace element during melting. For typical mantle oxygen fugacities ($f\text{O}_2$) carbon is stabilised in a reduced phase (either graphite or diamond) below the melting region (Dasgupta and Hirschmann, 2010). As mantle decompresses, mineral equilibria shift and cause the reduced carbon to be oxidised to carbonate (CO_3^{2-}). At typical mantle potential temperatures

this carbonate-bearing assemblage is above the carbonated peridotite solidus, meaning the transition is accompanied by ‘redox’ melting (Dasgupta and Hirschmann, 2010). Dilution of this melt by higher degree silicate melts is unavoidable; the carbon liberated from the residue by redox melting will have the apparent behaviour of an extremely incompatible element and therefore remain coupled to Ba and Nb.

If carbon abundances are sufficiently high to influence redox equilibria, or the mantle has anomalously low fO_2 , reduced carbon may persist into the melting region. In Appendix B we demonstrate that the presence of reduced carbon during melting will result in melts with extremely high CO_2/Ba ratios, and distinctive CO_2 -trace element systematics.

5.7. Global upper mantle CO_2 heterogeneity

Despite the unparalleled quantity of melt inclusion data available for Iceland, we are unable to place robust constraints on the carbon content of recycled mantle components. This limitation is due, in part, to having few eruptions constraining the mixing surface close to the EM-component. An alternative approach for assessing the effect of recycled material on the mantle CO_2 budget is to assess global variations in CO_2/Ba and CO_2/Nb ratios along the mid-ocean ridge system. The fairly uniform $R/R_a \sim 8$ for MORBs means the influence of primordial (high $^3He/^4He$ mantle) is excluded from the dataset. We also include eruptions from Iceland that have $R/R_a \sim 8$ (Borgarhraun and Berserkjakraun), in addition to Heilagsdalsfjall as nearby eruptions all have $R/R_a \sim 8$ (Harðardóttir et al., 2018), though He-isotope measurements have not been made on Heilagsdalsfjall material. Using the global dataset allows us to populate the DM–EM array with more depleted (but still variably enriched) eruptions, i.e., those which are less susceptible to CO_2 loss by magmatic degassing.

Figure 10 shows the compilation (filtered for eruptions with $R/R_a \sim 8$) of CO_2/Ba and CO_2/Nb ratios plotted against ratios used as indices of enrichment: $^{143}Nd/^{144}Nd$ (as used in Section 5.4), $^{206}Pb/^{204}Pb$ and Ba/Nb . Though not shown here, similar observations can be made with $^{207}Pb/^{204}Pb$, $^{208}Pb/^{204}Pb$ and $^{87}Sr/^{86}Sr$. Some caution must be exercised with comparing the radiogenic isotopes globally, as source age is convolved with enrichment in the isotope ratio values. As discussed in Section 1, we advocate taking the

highest values of CO_2/Ba and CO_2/Nb from melt inclusion datasets as the best proxy for the mantle, in preference to the dataset averages often used (Saal et al., 2002; Le Voyer et al., 2017; Hauri et al., 2018). In Figure 10 we highlight the difference between the two approaches for the datasets which preserve correlations between CO_2 and the trace elements (filled and unfilled blue circles). We distinguish melt inclusion datasets which do not retain a CO_2 -trace element correlation (orange circles) since they likely experienced greater extents and a more complex history of CO_2 degassing and magma mixing. CO_2 -undersaturated (ultra-depleted) MORB glasses are shown as grey circles.

Figures 10a, 10b and 10c show there is no systematic variation in CO_2/Ba with eruption enrichment. Likewise, Figures 10d and 10e show there is no covariation of CO_2/Nb with radiogenic isotope tracers of eruption enrichment, however a correlation is observed with Ba/Nb (Figure 10f). Hirschmann (2018) also described this feature in his compilation of global CO_2/Ba and CO_2/Nb ratios, though he found a stronger correlation between CO_2/Nb and Ba/Nb than shown here. This discrepancy arises since Hirschmann (2018) includes datasets associated with plumes (which we do not include as they may have contributions from high $^3He/^4He$ mantle) and presents the undersaturated glass measurements as a set of averages.

The highest CO_2/Ba ratios observed in datasets with CO_2 -trace element correlations coincide with the highest CO_2/Ba ratios seen in the undersaturated glasses, with the exception of the Garrett inclusions where the mean CO_2/Ba ratio observed in the melt inclusions is closest to the undersaturated glasses. The highest CO_2/Ba ratio measured in undersaturated glasses from the Siqueiros fracture zones (146 ± 31 , Michael and Graham, 2015) is intermediate between the mean and highest Siqueiros melt inclusion CO_2/Ba ratios (though it is within uncertainty of the highest inclusion value). This might suggest that the melts that were preserved as melt inclusions may have experienced some CO_2 loss, prior to homogenisation of the trace element and CO_2 enriched melts, and before mixing with depleted melts to form a binary mixing array with constant CO_2/Ba ratio (Matthews et al., 2017, Appendix A). Equally, the undersaturated glasses may reflect a subtly different mantle source. However, the coincidence of the mean CO_2/Ba ratio of the Garrett melt inclusions with the highest CO_2/Ba ratios observed in undersaturated glasses lends sup-

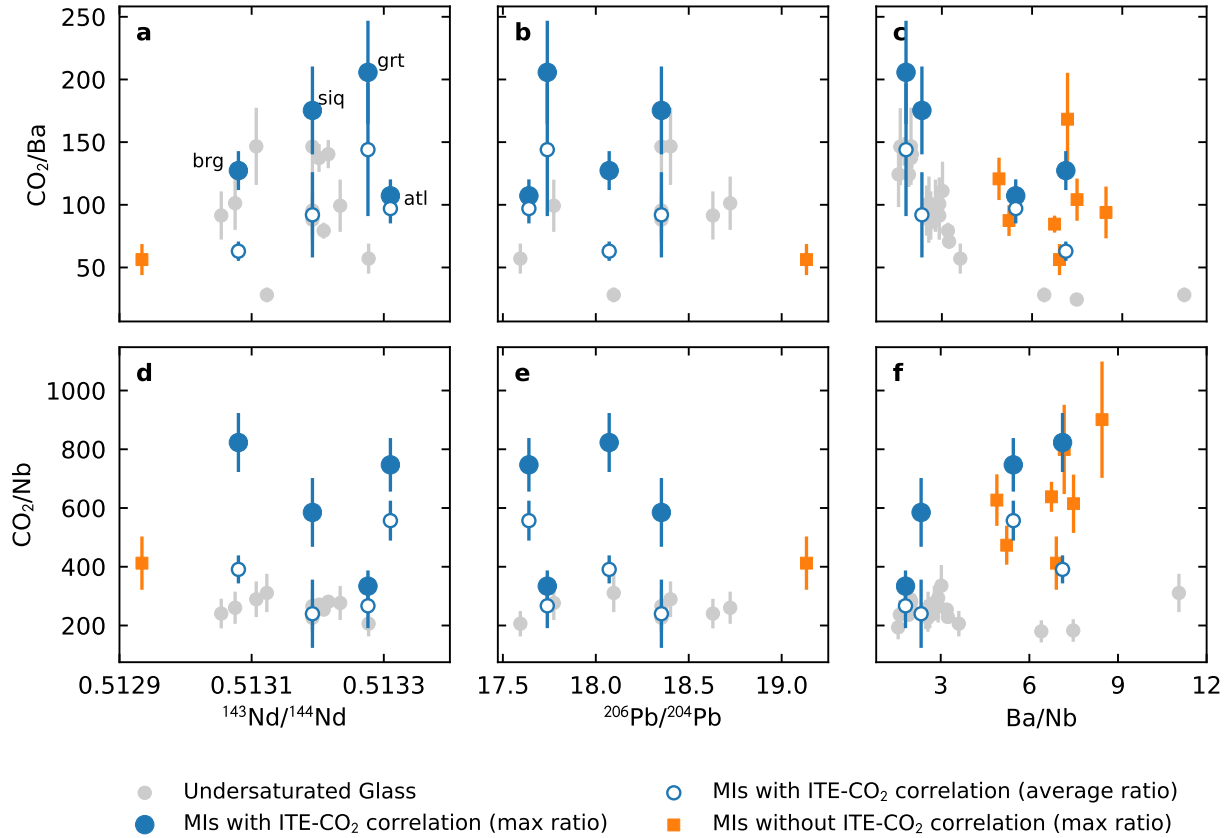


Figure 10: Compilation of data from the global spreading ridge system, filtered for $R/R_a \sim 8$. Melt inclusion datasets are separated into those exhibiting correlations between CO_2 and trace elements (blue circles), and those without a correlation (orange squares). For comparison we also show the CO_2/Ba and CO_2/Nb ratios that were reported for the datasets exhibiting correlations; these values were derived by taking dataset averages rather than by taking the maximum values as advocated here. Glasses that are undersaturated in CO_2 vapour at the pressure of eruption are shown as grey circles. The $^{143}\text{Nd}/^{144}\text{Nd}$, $^{206}\text{Pb}/^{204}\text{Pb}$ and Ba/Nb ratios for the melt inclusion datasets are taken from published analyses of whole-rock or matrix glass from the same eruptions, for which the sources are listed in Supplementary Table 3. The melt inclusion datasets with CO_2 -trace element correlations are labelled in Panel a (brg: Borgarhraun, siq: Siqueiros, grt: Garrett, atl: Equatorial Atlantic). The melt inclusion CO_2/Ba and CO_2/Nb ratios are reported by this study, Hauri et al. (2018); Le Voyer et al. (2017); Shimizu et al. (2019); Helo et al. (2011); Wanless and Shaw (2012); Wanless et al. (2014). The undersaturated glass CO_2/Ba and CO_2/Nb ratios were reported by Shimizu et al. (2016); Michael and Graham (2015).

port to the argument of (Shimizu et al., 2019); that the Garrett melt inclusions represent a rare case of the inclusions preserving largely undegassed melts.

Most of the datasets without a CO₂-trace element correlation have CO₂/Ba ratios lower than datasets with a correlation, this could reflect a greater extent of CO₂ degassing and mixing seen by the datasets that lack a correlation. The undersaturated glasses have CO₂/Ba ratios that overlap with the range displayed by the melt inclusion datasets. The lowest CO₂/Ba ratios (<50) seen in the undersaturated glasses are significantly lower than the CO₂/Ba ratios seen in melt inclusion datasets at similar Ba/Nb. Matthews et al. (2017) demonstrated that undersaturation at eruption cannot be taken as evidence that CO₂ has not been lost; the undersaturated nature of the glasses may come from mixing of melts undersaturated in CO₂ vapour with melts that saturated in CO₂ vapour during magma storage. We therefore think it most likely that the undersaturated glasses with lowest CO₂/Ba lost substantial CO₂ vapour during magma storage.

The strength of the correlation between CO₂/Nb and Ba/Nb shown in Figure 10f arises from the low CO₂/Nb ratios associated with the samples with low Ba/Nb. The low Ba/Nb samples are from eruptions in fracture zones, including the melt inclusion datasets from the Garrett and Siqueiros fracture zones (Shimizu et al., 2019). Hirschmann (2018) suggests that the correlation may arise from Nb being fractionated from Ba and CO₂ during mantle melting. Whilst we have shown that Nb and Ba are not fractionated from each other during the melting processes that generated the Iceland melt inclusion suites (Section 3.2); the same is not true of Siqueiros. Supplementary Figure 18 demonstrates that the Ba/Nb ratio of the Siqueiros inclusions increases with Ba concentration, and the normalised variances of Ba and Nb differ, both observations that suggest Ba and Nb have been fractionated from each other during melting. However, CO₂ and Ba have comparable normalised variance, suggesting that they are sufficiently incompatible that they haven't been fractionated from one another and that the CO₂/Ba ratio should therefore have been largely unaffected by the melting process.

Michael and Graham (2015) suggested that ultra-depleted glasses are generated where melt aggregation is incomplete, with a particularly low contribution from the deepest melts. This partial aggregation provides a mechanism for fractionating Nb from Ba and CO₂ that is likely to only occur in

fracture zones, and therefore may explain the origin of the low CO₂/Nb and Ba/Nb population in Figure 10. If fracture-zone eruptions (low Ba/Nb) are discounted from Figure 10, a correlation remains between Ba/Nb and CO₂/Nb, though it is weaker. Given that Ba and Nb have not been fractionated from each other during melting in the petrogenesis of these non-fracture zone eruptions, this correlation is most likely a source feature and may reflect a decoupling of Nb and Ba concentrations during recycling (Hirschmann, 2018).

As discussed in Section 5.3, it is possible that the variation in ¹⁴³Nd/¹⁴⁴Nd observed between Icelandic eruptions is decoupled from CO₂/Ba and CO₂/Nb by melt transport, and so our proxy for source components could be invalid. A more reliable record of the local mantle average Nd-, Sr- and Pb-isotope ratios is ridge-segment average values (Shorttle, 2015). Supplementary Figure 19 nonetheless demonstrates that CO₂/Ba and CO₂/Nb do not co-vary with ridge-segment average Nd- and Pb-isotope ratios.

6. Whole mantle CO₂ mass balance

In Section 5.4.2 we demonstrated that reasonable constraints may be placed on the CO₂ concentration in a depleted mantle component (DM) and a primordial component (PM) in Iceland, but there is little constraint on the CO₂ content in the recycled mantle component (EM). In Section 5.7 we showed that there is little variation in the CO₂/Ba ratio with degree of enrichment in the upper mantle. If the variable enrichment of the upper mantle is primarily controlled by varying amounts of recycled material (e.g. Chauvel et al., 2008) this might be taken to suggest there is little difference in the CO₂/Ba ratio of the depleted mantle and recycled mantle.

Marty (2012) estimated a whole mantle averaged CO₂ concentration of 2130±1390 ppmw. By making the approximation that the whole mantle can be described as a mixture of the three mantle components, DM, EM, and PM, we inverted for using the Iceland data, we can assess the range of EM CO₂ concentrations that are consistent with the bulk mantle CO₂ estimate made by Marty (2012). Since the relative proportions of the three components are poorly known we allow them each to vary from 0–100%.

Figure 11 shows the CO₂ concentration of the EM component required to satisfy this mass balance, as

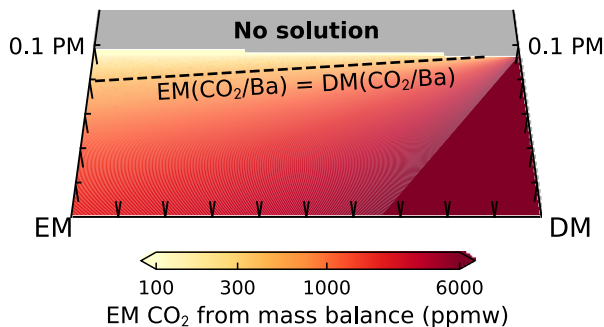


Figure 11: The concentration of CO₂ required in the EM component to satisfy mass balance assuming a bulk mantle CO₂ concentration of 2130 ppmw (Marty, 2012), plotted here in a ternary diagram of mass fraction. The calculation assumes the DM mantle component has 102 ppmw CO₂, and the PM component has 2.2 wt%. The dashed line indicates the locus of solutions where the EM and DM components have the same CO₂/Ba ratio, assuming a Ba concentration of 0.563 ppmw in the DM component, and 2.55 ppmw in the EM component (Table 1).

a function of the relative proportions of DM, EM and PM in the whole mantle. In the calculation the CO₂ content of the DM and PM components is taken as the median value of their respective posterior distributions from Section 5.4.2. If the depleted mantle and enriched mantle have the same CO₂/Ba ratio, 8–10% of the mantle must be primordial to satisfy this mass balance.

The large low shear velocity provinces (LLSVPs) near the base of the mantle have been suggested to host primordial geochemical signatures (Castillo, 1988), though these account for only 2% of the mantle’s volume (Hernlund and Houser, 2008). Whilst the LLSVPs may be too small to host the required mass of carbon, mass-balance calculations using lithophile elements suggest up to 50% of the mantle might be primordial (Turcotte et al., 2001). Having 10% of the mantle bearing primordial high CO₂ concentrations is, therefore, perhaps not unreasonable. Further support comes from 2D mantle convection models; Ballmer et al. (2017) demonstrated that 10–15% of the mantle could remain isolated from convection if those domains are anomalously rich in bridgmanite.

7. Conclusions

We have leveraged a large new melt inclusion dataset of trace element and CO₂ concentrations

in geochemically diverse Icelandic eruptions, alongside existing suites of melt inclusions, to place new constraints on the interplay of source and process on CO₂/Ba and CO₂/Nb ratios. The key results are:

1. Though there is a global covariation of CO₂/Ba with enrichment in melt inclusions, this is a result of olivine decrepitation limiting the CO₂ concentration in melt inclusions. Decrepitation may be avoided if a significant fraction of a melt inclusion’s CO₂ budget is partitioned into a vapour bubble. When the CO₂ contained in vapour bubbles is added back into their coexisting glass, substantial heterogeneity in CO₂/Ba between Icelandic eruptions remains.
2. The maximum CO₂/Ba and CO₂/Nb values within Icelandic melt inclusion datasets co-vary with radiogenic isotope proxies for the contributions of depleted, primordial and enriched mantle components to the melts. The highest CO₂/Ba and CO₂/Nb are associated with primordial mantle derived melts, and the lowest with enriched mantle derived melts. Whilst it is likely the low CO₂/Ba and CO₂/Nb associated with the enriched mantle is due to the greater tendency for enriched melts to be affected by degassing, we argue the elevated CO₂/Ba and CO₂/Nb ratios for primordial mantle derived melts relative to depleted mantle is a consequence of elevated CO₂ in the solid primordial mantle.
3. Using the observed covariation of CO₂/Ba and CO₂/Nb with mantle source we invert for the CO₂ concentration in the Icelandic mantle sources, and find concentrations of 102^{+53}_{-27} ppmw for the depleted mantle, $2.2^{+3.8}_{-1.5}$ wt% for the primordial mantle, and 67^{+22000}_{-67} ppmw for the enriched/recycled mantle. Though the CO₂ concentration is likely to be greater in the enriched mantle than the depleted mantle, this could correspond to similar CO₂/Ba and CO₂/Nb ratios in both sources.
4. The global mid-ocean ridge CO₂/Ba and CO₂/Nb observations show no systematic variation of CO₂/Ba with enrichment, but do show a variation in CO₂/Nb with Ba/Nb ratio; these observations may suggest similar behaviour of Ba and CO₂ during recycling, but different behaviour of Nb.
5. Our new estimates of mantle source CO₂ con-

centrations are consistent with estimates of the total quantity of CO₂ in the mantle.

8. Acknowledgements

The authors wish to thank Rob Clarke, Martin Walker and Chris Parish for their assistance with sample preparation, Sébastien Facq for his help with operating the Raman instrument, Iris Buisman for her help with the SEM and EPMA measurements, and Richard Hinton for his help with the SIMS analyses. Helen Williams is thanked for commenting on an early version of the manuscript. Calcium Reekie is thanked for helpful discussions. The figures used in this paper were generated with the matplotlib and basemap python packages (Hunter, 2007). Data reduction was performed using the numpy (Oliphant, 2006) and pandas (McKinney, 2010) python packages. The authors would like to thank the Isaac Newton Institute for Mathematical Sciences for its hospitality during the programme ‘Melt in the Mantle’, which was supported by EPSRC Grant Number EP/K032208/1. SM was supported by a Natural Environment Research Council Studentship NE/L002507/1 and NE/M000427/1. JFR thanks the Leverhulme Trust.

References

- Aigner-Torres, M., Blundy, J., Ulmer, P., Pettke, T., 2007. Laser ablation ICPMS study of trace element partitioning between plagioclase and basaltic melts: an experimental approach. *Contributions to Mineralogy and Petrology* 153 (6), 647–667.
- Allison, C. M., Roggensack, K., Clarke, A. B., 2019. H₂O–CO₂ solubility in alkali-rich mafic magmas: new experiments at mid-crustal pressures. *Contributions to Mineralogy and Petrology* 174 (7), 58.
- Anderson, K. R., Poland, M. P., 2017. Abundant carbon in the mantle beneath Hawai‘i. *Nature Geoscience* 10 (9), 704.
- Bali, E., Hartley, M., Halldórsson, S., Gudfinnsson, G., Jakobsson, S., 2018. Melt inclusion constraints on volatile systematics and degassing history of the 2014–2015 Holuhraun eruption, Iceland. *Contributions to Mineralogy and Petrology* 173 (2), 9.
- Ballmer, M. D., Houser, C., Hernlund, J. W., Wentzcovitch, R. M., Hirose, K., 2017. Persistence of strong silica-enriched domains in the Earth’s lower mantle. *Nature Geoscience* 10 (3), 236.
- Berry, A. J., Stewart, G. A., O’Neill, H. S. C., Mallmann, G., Mosselmans, J. F. W., 2018. A re-assessment of the oxidation state of iron in MORB glasses. *Earth and Planetary Science Letters* 483, 114–123.
- Bouidoire, G., Rizzo, A. L., Di Muro, A., Grassa, F., Liuzzo, M., 2018. Extensive CO₂ degassing in the upper mantle beneath oceanic basaltic volcanoes: First insights from Piton de la Fournaise volcano (La Réunion Island). *Geochimica et Cosmochimica Acta* 235, 376–401.
- Buchner, J., Georgakakis, A., Nandra, K., Hsu, L., Rangel, C., Brightman, M., Merloni, A., Salvato, M., Donley, J., Kocevski, D., 2014. X-ray spectral modelling of the AGN obscuring region in the CDFS: Bayesian model selection and catalogue. *Astronomy & Astrophysics* 564, A125.
- Cabral, R. A., Jackson, M. G., Koga, K. T., Rose-Koga, E. F., Hauri, E. H., Whitehouse, M. J., Price, A. A., Day, J., Shimizu, N., Kelley, K. A., 2014. Volatile cycling of H₂O, CO₂, F, and Cl in the HIMU mantle: A new window provided by melt inclusions from oceanic hot spot lavas at Mangaia, Cook Islands. *Geochemistry, Geophysics, Geosystems* 15 (11), 4445–4467.
- Cartigny, P., Pineau, F., Aubaud, C., Javoy, M., 2008. Towards a consistent mantle carbon flux estimate: Insights from volatile systematics (H₂O/Ce, δD, CO₂/Nb) in the north atlantic mantle (14°N and 34°N). *Earth and Planetary Science Letters* 265 (3–4), 672–685.
- Castillo, P., 1988. The Dupal anomaly as a trace of the upwelling lower mantle. *Nature* 336 (6200), 667.
- Chauvel, C., Lewin, E., Carpentier, M., Arndt, N. T., Marini, J.-C., 2008. Role of recycled oceanic basalt and sediment in generating the Hf–Nd mantle array. *Nature geoscience* 1 (1), 64.
- Class, C., Goldstein, S. L., 2005. Evolution of helium isotopes in the Earth’s mantle. *Nature* 436 (7054), 1107.
- Cottrell, E., Kelley, K. A., 2011. The oxidation state of Fe in MORB glasses and the oxygen fugacity of the upper mantle. *Earth and Planetary Science Letters* 305 (3), 270–282.
- Dasgupta, R., Hirschmann, M. M., 2010. The deep carbon cycle and melting in earth’s interior. *Earth and Planetary Science Letters* 298 (1–2), 1–13.
- Dixon, J. E., 1997. Degassing of alkalic basalts. *American Mineralogist* 82 (3–4), 368–378.
- Dixon, J. E., Stolper, E. M., Holloway, J. R., 1995. An experimental study of water and carbon dioxide solubilities in mid-ocean ridge basaltic liquids. Part I: calibration and solubility models. *Journal of Petrology* 36 (6), 1607–1631.
- Duncan, M. S., Dasgupta, R., Tsuno, K., 2017. Experimental determination of CO₂ content at graphite saturation along a natural basalt-peridotite melt join: Implications for the fate of carbon in terrestrial magma oceans. *Earth and Planetary Science Letters* 466, 115–128.
- Eguchi, J., Dasgupta, R., 2018a. A CO₂ solubility model for silicate melts from fluid saturation to graphite or diamond saturation. *Chemical Geology* 487, 23–38.
- Eguchi, J., Dasgupta, R., 2018b. Redox state of the convective mantle from CO₂-trace element systematics of oceanic basalts. *Geochemical Perspectives Letters* 8.
- Feroz, F., Hobson, M., 2008. Multimodal nested sampling: an efficient and robust alternative to Markov Chain Monte Carlo methods for astronomical data analyses. *Monthly Notices of the Royal Astronomical Society* 384 (2), 449–463.
- Feroz, F., Hobson, M., Bridges, M., 2009. Multinest: an efficient and robust bayesian inference tool for cosmology and particle physics. *Monthly Notices of the Royal Astronomical Society* 398 (4), 1601–1614.
- Feroz, F., Hobson, M., Cameron, E., Pettitt, A., 2013. Importance nested sampling and the MultiNest algorithm. arXiv preprint arXiv:1306.2144.
- Harðardóttir, S., Halldórsson, S. A., Hilton, D. R., 2018. Spatial distribution of helium isotopes in Icelandic

- geothermal fluids and volcanic materials with implications for location, upwelling and evolution of the Icelandic mantle plume. *Chemical Geology* 480, 12–27.
- Hart, S. R., Hauri, E. H., Oschmann, L. A., Whitehead, J. A., 1992. Mantle plumes and entrainment: Isotopic evidence. *Science* 256 (5056), 517–520.
- Hartley, M. E., MacLennan, J., Edmonds, M., Thordarson, T., 2014. Reconstructing the deep CO₂ degassing behaviour of large basaltic fissure eruptions. *Earth and Planetary Science Letters* 393, 120–131.
- Hauri, E. H., MacLennan, J., McKenzie, D., Gronvold, K., Oskarsson, N., Shimizu, N., 2018. CO₂ content beneath northern Iceland and the variability of mantle carbon. *Geology* 46 (1), 55–58.
- Heber, V. S., Brooker, R. A., Kelley, S. P., Wood, B. J., 2007. Crystal–melt partitioning of noble gases (helium, neon, argon, krypton, and xenon) for olivine and clinopyroxene. *Geochimica et Cosmochimica Acta* 71 (4), 1041–1061.
- Helo, C., Longpré, M.-A., Shimizu, N., Clague, D. A., Stix, J., 2011. Explosive eruptions at mid-ocean ridges driven by CO₂-rich magmas. *Nature Geoscience* 4 (4), 260.
- Hernlund, J. W., Houser, C., 2008. On the statistical distribution of seismic velocities in Earth’s deep mantle. *Earth and Planetary Science Letters* 265 (3-4), 423–437.
- Hirschmann, M. M., 2018. Comparative deep earth volatile cycles: The case for C recycling from exosphere/mantle fractionation of major (H₂O, C, N) volatiles and from H₂O/Ce, CO₂/Ba, and CO₂/Nb exosphere ratios. *Earth and Planetary Science Letters*.
- Hjartarson, Á., Sæmundsson, K., 2014. Geological map of Iceland, bedrock. 1: 600,000. Iceland GeoSurvey, Reykjavík.
- Iacono-Marziano, G., Morizet, Y., Le Trong, E., Gaillard, F., 2012. New experimental data and semi-empirical parameterization of H₂O–CO₂ solubility in mafic melts. *Geochimica et Cosmochimica Acta* 97, 1–23.
- Jackson, M. G., Kurz, M. D., Hart, S. R., Workman, R. K., 2007. New Samoan lavas from Ofu island reveal a hemispherically heterogeneous high ³He/⁴He mantle. *Earth and Planetary Science Letters* 264 (3-4), 360–374.
- Jones, M., Wanless, V., Soule, S., Kurz, M., Mittelstaedt, E., Fornari, D., Curtice, J., Klein, F., Le Roux, V., Brodsky, H., et al., 2019. New constraints on mantle carbon from Mid-Atlantic Ridge popping rocks. *Earth and Planetary Science Letters* 511, 67–75.
- Kelemen, P., Hirth, G., Shimizu, N., Spiegelman, M., Dick, H., 1997. A review of melt migration processes in the adiabatically upwelling mantle beneath oceanic spreading ridges. *Philosophical Transactions of the Royal Society of London A: Mathematical, Physical and Engineering Sciences* 355 (1723), 283–318.
- Kelemen, P. B., Manning, C. E., 2015. Reevaluating carbon fluxes in subduction zones, what goes down, mostly comes up. *Proceedings of the National Academy of Sciences*, 201507889.
- Kerrick, D., Connolly, J., 2001. Metamorphic devolatilization of subducted oceanic metabasalts: implications for seismicity, arc magmatism and volatile recycling. *Earth and Planetary Science Letters* 189 (1-2), 19–29.
- Kurz, M., Jenkins, W., 1981. The distribution of helium in oceanic basalt glasses. *Earth and Planetary Science Letters* 53 (1), 41–54.
- Le Voyer, M., Kelley, K., Cottrell, E., Hauri, E., 2017. Heterogeneity in mantle carbon content from CO₂-undersaturated basalts. *Nature communications* 8, 14062.
- Lee, P. M., 2012. Bayesian statistics: an introduction. John Wiley & Sons.
- MacLennan, J., 2008a. Concurrent mixing and cooling of melts under Iceland. *Journal of Petrology* 49 (11), 1931–1953.
- MacLennan, J., 2008b. Lead isotope variability in olivine-hosted melt inclusions from Iceland. *Geochimica et Cosmochimica Acta* 72 (16), 4159–4176.
- MacLennan, J., 2017. Bubble formation and decrepitation control the CO₂ content of olivine-hosted melt inclusions. *Geochemistry, Geophysics, Geosystems* 18 (2), 597–616.
- Marty, B., 2012. The origins and concentrations of water, carbon, nitrogen and noble gases on earth. *Earth and Planetary Science Letters* 313, 56–66.
- Matthews, S., Shorttle, O., Rudge, J. F., MacLennan, J., 2017. Constraining mantle carbon: CO₂-trace element systematics in basalts and the roles of magma mixing and degassing. *Earth and Planetary Science Letters* 480, 1–14.
- Métrich, N., Zanon, V., Créon, L., Hildenbrand, A., Moreira, M., Marques, F. O., 2014. Is the ‘Azores hotspot’ a wetspot? insights from the geochemistry of fluid and melt inclusions in olivine of Pico basalts. *Journal of Petrology* 55 (2), 377–393.
- Michael, P. J., Graham, D. W., 2015. The behavior and concentration of CO₂ in the suboceanic mantle: inferences from undegassed ocean ridge and ocean island basalts. *Lithos* 236, 338–351.
- Miller, W. G., MacLennan, J., Shorttle, O., Gaetani, G. A., Le Roux, V., Klein, F., 2019. Estimating the carbon content of the deep mantle with Icelandic melt inclusions. *Earth and Planetary Science Letters* 523, 115699.
- Neave, D. A., MacLennan, J., Edmonds, M., Thordarson, T., 2014. Melt mixing causes negative correlation of trace element enrichment and CO₂ content prior to an Icelandic eruption. *Earth and Planetary Science Letters* 400, 272–283.
- Neave, D. A., Putirka, K. D., 2017. A new clinopyroxene-liquid barometer, and implications for magma storage pressures under Icelandic rift zones. *American Mineralogist* 102 (4), 777–794.
- Neave, D. A., Shorttle, O., Oeser, M., Weyer, S., Kobayashi, K., 2018. Mantle-derived trace element variability in olivines and their melt inclusions. *Earth and Planetary Science Letters* 483, 90–104.
- Palme, H., O’Neill, H. S. C., 2003. Cosmochemical estimates of mantle composition. *Treatise on geochemistry* 2, 568.
- Peate, D. W., Breddam, K., Baker, J. A., Kurz, M. D., Barker, A. K., Prestvik, T., Grassineau, N., Skovgaard, A. C., 2010. Compositional characteristics and spatial distribution of enriched Icelandic mantle components. *Journal of Petrology* 51 (7), 1447–1475.
- Rosenthal, A., Hauri, E., Hirschmann, M., 2015. Experimental determination of C, F, and H partitioning between mantle minerals and carbonated basalt, CO₂/Ba and CO₂/Nb systematics of partial melting, and the CO₂ contents of basaltic source regions. *Earth and Planetary Science Letters* 412, 77–87.
- Rudge, J. F., MacLennan, J., Stracke, A., 2013. The geochemical consequences of mixing melts from a heterogeneous mantle. *Geochimica et Cosmochimica Acta* 114, 112–143.
- Saal, A. E., Hauri, E. H., Langmuir, C. H., Perfit, M. R., 2002. Vapour undersaturation in primitive mid-ocean-ridge basalt and the volatile content of earth’s upper mantle. *Nature* 419 (6906), 451.

- Sæmundsson, K., Hjartarson, Á., Kaldal, I., Sigurgeirsson, M., Kristinsson, S., Vikingsson, S., 2012. Geological map of the northern volcanic zone, Iceland. Northern part 1 (100.000).
- Sæmundsson, K., Jóhannesson, H., Hjartarson, Á., Kristinsson, S. G., Sigurgeirsson, M., 2010. Geological map of southwest Iceland, 1: 100.000. Iceland GeoSurvey.
- Schipper, C. I., Le Voyer, M., Moussallam, Y., White, J. D., Thordarson, T., Kimura, J.-I., Chang, Q., 2016. Degassing and magma mixing during the eruption of surtsey volcano (Iceland, 1963–1967): the signatures of a dynamic and discrete rift propagation event. *Bulletin of Volcanology* 78 (4), 33.
- Shimizu, K., Saal, A. E., Hauri, E. H., Perfit, M. R., Hékinian, R., 2019. Evaluating the roles of melt-rock interaction and partial degassing on the CO₂/Ba ratios of MORB: implications for the CO₂ budget in the Earth–Åž depleted upper mantle. *Geochimica et Cosmochimica Acta*.
- Shimizu, K., Saal, A. E., Myers, C. E., Nagle, A. N., Hauri, E. H., Forsyth, D. W., Kamenetsky, V. S., Niu, Y., 2016. Two-component mantle melting-mixing model for the generation of mid-ocean ridge basalts: implications for the volatile content of the Pacific upper mantle. *Geochimica et Cosmochimica Acta* 176, 44–80.
- Shishkina, T. A., Botcharnikov, R. E., Holtz, F., Almeev, R. R., Jazwa, A. M., Jakubiak, A. A., 2014. Compositional and pressure effects on the solubility of H₂O and CO₂ in mafic melts. *Chemical Geology* 388, 112–129.
- Shorttle, O., 2015. Geochemical variability in MORB controlled by concurrent mixing and crystallisation. *Earth and Planetary Science Letters* 424, 1–14.
- Shorttle, O., MacLennan, J., 2011. Compositional trends of icelandic basalts: Implications for short-length scale lithological heterogeneity in mantle plumes. *Geochemistry, Geophysics, Geosystems* 12 (11).
- Shorttle, O., MacLennan, J., Piotrowski, A. M., 2013. Geochemical provincialism in the Iceland plume. *Geochimica et Cosmochimica Acta* 122, 363–397.
- Shorttle, O., Moussallam, Y., Hartley, M. E., MacLennan, J., Edmonds, M., Murton, B. J., 2015. Fe-XANES analyses of Reykjanes Ridge basalts: Implications for oceanic crust’s role in the solid Earth oxygen cycle. *Earth and Planetary Science Letters* 427, 272–285.
- Shorttle, O., Rudge, J. F., MacLennan, J., Rubin, K. H., 2016. A statistical description of concurrent mixing and crystallization during MORB differentiation: implications for trace element enrichment. *Journal of Petrology* 57 (11–12), 2127–2162.
- Sides, I., Edmonds, M., MacLennan, J., Swanson, D., Houghton, B., 2014. Eruption style at Kilauea volcano in Hawai’i linked to primary melt composition. *Nature Geoscience* 7 (6), 464.
- Skovgaard, A. C., Storey, M., Baker, J., Blusztajn, J., Hart, S. R., 2001. Osmium–oxygen isotopic evidence for a recycled and strongly depleted component in the Iceland mantle plume. *Earth and Planetary Science Letters* 194 (1), 259–275.
- Sobolev, A., 1996. Melt inclusions in minerals as a source of principle petrological information. *Petrology* 4 (3), 209–220.
- Sobolev, A., Shimizu, N., 1993. Ultra-depleted primary melt included in an olivine from the mid-atlantic ridge. *Nature* 363 (6425), 151.
- Sohn, R. A., 2013. A method for inverting ratio–ratio data to estimate end-member compositions in mixing problems. *Chemical Geology* 352, 63–69.
- Spiegelman, M., Kelemen, P. B., 2003. Extreme chemical variability as a consequence of channelized melt transport. *Geochemistry, Geophysics, Geosystems* 4 (7).
- Stolper, E., Holloway, J. R., 1988. Experimental determination of the solubility of carbon dioxide in molten basalt at low pressure. *Earth and Planetary Science Letters* 87 (4), 397–408.
- Stracke, A., Bizimis, M., Salters, V. J., 2003. Recycling oceanic crust: Quantitative constraints. *Geochemistry, Geophysics, Geosystems* 4 (3).
- Stracke, A., Hofmann, A. W., Hart, S. R., 2005. FOZO, HIMU, and the rest of the mantle zoo. *Geochemistry, Geophysics, Geosystems* 6 (5).
- Stuart, F. M., Lass-Evans, S., Fitton, J. G., Ellam, R. M., 2003. High ³he/⁴he ratios in picritic basalts from Baffin island and the role of a mixed reservoir in mantle plumes. *Nature* 424 (6944), 57.
- Su, Y., 2003. Global MORB chemistry compilation at the segment scale. Ph. D. Thesis, Department of Earth and Environmental Sciences, Columbia University.
- Thirlwall, M., Gee, M., Taylor, R., Murton, B., 2004. Mantle components in iceland and adjacent ridges investigated using double-spike Pb isotope ratios. *Geochimica et Cosmochimica Acta* 68 (2), 361–386.
- Trull, T., Nadeau, S., Pineau, F., Polve, M., Javoy, M., 1993. C-He systematics in hotspot xenoliths: Implications for mantle carbon contents and carbon recycling. *Earth and Planetary Science Letters* 118 (1–4), 43–64.
- Tucker, J. M., Hauri, E. H., Pietruszka, A. J., Garcia, M. O., Marske, J. P., Trusdell, F. A., 2019. A high carbon content of the Hawaiian mantle from olivine-hosted melt inclusions. *Geochimica et Cosmochimica Acta* 254, 156–172.
- Tucker, J. M., Mukhopadhyay, S., Gonnermann, H. M., 2018. Reconstructing mantle carbon and noble gas contents from degassed mid-ocean ridge basalts. *Earth and Planetary Science Letters* 496, 108–119.
- Turcotte, D., Paul, D., White, W., 2001. Thorium-uranium systematics require layered mantle convection. *Journal of Geophysical Research: Solid Earth* 106 (B3), 4265–4276.
- Wanamaker, B., Wong, T.-F., Evans, B., 1990. Decrepitation and crack healing of fluid inclusions in San Carlos olivine. *Journal of Geophysical Research: Solid Earth* 95 (B10), 15623–15641.
- Wanless, V., Behn, M., Shaw, A., Plank, T., 2014. Variations in melting dynamics and mantle compositions along the Eastern Volcanic Zone of the Gakkel Ridge: insights from olivine-hosted melt inclusions. *Contributions to Mineralogy and Petrology* 167 (5), 1005.
- Wanless, V. D., Shaw, A. M., 2012. Lower crustal crystallization and melt evolution at mid-ocean ridges. *Nature Geoscience* 5 (9), 651.
- Wanless, V. D., Shaw, A. M., Behn, M. D., Soule, S. A., Escartin, J., Hamelin, C., 2015. Magmatic plumbing at Lucky Strike volcano based on olivine-hosted melt inclusion compositions. *Geochemistry, Geophysics, Geosystems* 16 (1), 126–147.
- Wasson, J. T., Kallemeyn, G. W., 1988. Compositions of chondrites. *Philosophical Transactions of the Royal Society of London. Series A, Mathematical and Physical Sciences* 325 (1587), 535–544.
- Wippeny, B., MacLennan, J., 2011. A partial record of mixing of mantle melts preserved in icelandic phenocrysts. *Journal of Petrology* 52 (9), 1791–1812.

Workman, R. K., Hart, S. R., 2005. Major and trace element composition of the depleted MORB mantle (DMM). *Earth and Planetary Science Letters* 231 (1), 53–72.

Appendix A. Bubble corrections without CO₂ vapour density measurements

The bubble corrections applied to the melt inclusions in this study are all derived from observations of the CO₂ vapour density in the bubble. An alternative approach that has been used, for example in the Borgarhraun dataset by Hauri et al. (2018), is to calculate the CO₂ vapour density that would have been in equilibrium with the melt at the glass transition temperature. However, this assumes that diffusion of CO₂ through the inclusion was not kinetically limited. Neave et al. (2014) made comprehensive observations to show that any CO₂ present in the bubbles within melt inclusions from the Skuggafjöll eruption must be below detection limit, despite significant CO₂ concentrations within the glass. We therefore believe that such corrections must be regarded with great caution.

The variance structure of the Borgarhraun melt inclusions analysed by Hauri et al. (2018) is shown in Figure A.1a. The positive trend between $1/\sqrt{D}$ and the normalised standard deviation (σ/μ) for elements more incompatible than Nb is consistent with them being fractionated from each other by fractional melting. The plateau defined by Nb, Th, U, Ba and Rb, suggests these elements were not fractionated from each other during fractional melting. Uncorrected CO₂ sits below this plateau, indicating the variance in CO₂ concentration has been reduced, most likely by partial degassing. When the bubble-corrected CO₂ concentrations are used instead (shown by the red CO₂^{*}) the variance is higher than expected, given the variance of similarly compatible elements. For comparison, Supplementary Figure 3 shows similar plots for the data presented here. Berserkjahraun and Stapafell also have CO₂^{*} with a greater variance than expected. However, Berserkjahraun is most likely to have significant under-corrections for the CO₂ it has lost (see main text for discussion) and so this enhanced variance most likely represents scatter from variably incomplete correction. The uncorrected CO₂ concentrations from Stapafell also have a higher than expected variance, this is most likely to be generated by the melt inclusions preserving two stages of partial degassing and mixing. Borgarhraun has

much simpler CO₂-trace element systematics, suggesting a single stage degassing and mixing process. This is supported by the correlation coefficients between $1/El$ and CO₂/El (where El is the concentration of a trace element) shown in Figure A.1b. If CO₂ were behaving identically to a trace element, and had not undergone partial degassing and mixing, the correlation coefficient should rapidly decrease at the partition coefficient for CO₂, shown by the vertical dashed line (Matthews et al., 2017). The calculated correction should not give an incomplete correction, and so it is most likely that the elevated variance arises from over-correcting the CO₂ concentrations. We therefore omit these corrected values from the analysis presented here.

Appendix B. Graphite Saturated Melting

The calculations of melt CO₂ concentrations in the main text are valid only if carbon is present only as a trace element or as carbonate in the solid mantle. The stability of carbonate over graphite is controlled by the oxygen fugacity (fO_2) of the mantle (e.g. Dasgupta and Hirschmann, 2010). Eguchi and Dasgupta (2018b) modelled the CO₂/Ba ratios of basalts with contributions from a graphite-saturated mantle source. They concluded that such models provide a poor fit to natural MORB and OIB, thereby inferring that graphite-saturated melts do not generally contribute to basaltic volcanism. By incorporating graphite saturation into the model used by Matthews et al. (2017) we extend the work of Eguchi and Dasgupta (2018b) by assessing how the signal of graphite-saturated melts might be modulated by the mixing and degassing processes.

The CO₂ content of the melt at graphite saturation was calculated as a function of melt composition and fO_2 using the formulation of Duncan et al. (2017). Once graphite is exhausted, we assume CO₂ is entirely depleted from the solid residue. To maintain consistency with other trace elements, which we model as melting continuously, we allow for CO₂ to remain within the residual porosity with a growing degree of dilution and assuming perfectly incompatible behaviour.

For a single melting increment of dF_n with a residual porosity of ϕ :

$$C_n = \frac{\phi - dF_n}{\phi} C_{n-1} \quad (\text{B.1})$$

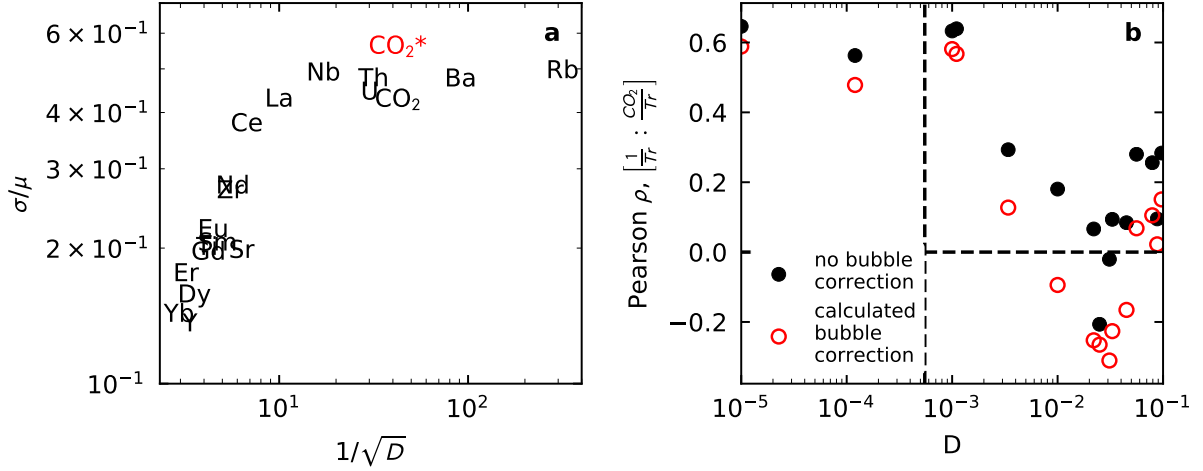


Figure A.1: Panel a shows the variance structure of the Borgarhraun dataset. The standard deviation normalised to the mean for each trace element is shown as a function of its partition coefficient (D) as reported by Workman and Hart (2005). CO_2^* indicates bubble-corrected CO_2 concentrations. Panel b shows the Pearson correlation coefficient for $1/\text{El}$ vs CO_2/El (where El is a trace element), as used by Matthews et al. (2017). The vertical dashed line shows the partition coefficient of CO_2 during melting as determined by Rosenthal et al. (2015).

where C_n and $C_{(n-1)}$ are the CO_2 concentrations in the residual porosity after, and before the n th melting increment, respectively. This can be applied recursively to yield:

$$C_n = \left[\frac{\phi - dF_n}{\phi} \right] \left[\frac{\phi - dF_{n-1}}{\phi} \right] \dots \left[\frac{\phi - dF_1}{\phi} \right] C_0 \quad (\text{B.2})$$

$$C_n = \frac{C_0}{\phi^n} \prod_{i=0}^{n-1} \phi - dF_{n-i} \quad (\text{B.3})$$

where C_0 is the CO_2 concentration in the melt at the point of graphite exhaustion. Setting $dF_{n+1} = dF_n = dF$,

$$C_n = C_0 \left(1 - \frac{dF}{\phi} \right)^n \quad (\text{B.4})$$

and since:

$$dF = \frac{\Delta F}{n} \quad (\text{B.5})$$

where $\Delta F = F - F_{\text{graphite-exhaustion}}$, the concentration at a given ΔF may be written:

$$C(\Delta F) = C_0 \left(1 - \frac{\Delta F}{\phi n} \right)^n \quad (\text{B.6})$$

in the limit $dF \rightarrow 0$ and $n \rightarrow \infty$:

$$C(\Delta F) = C_0 e^{-\frac{\Delta F}{\phi}} \quad (\text{B.7})$$

Examples of these calculations for variable $f\text{O}_2$, are shown in Figure B.2. Graphite saturation during melting decreases the CO_2 content of the most enriched melts, and increases the CO_2 concentration in the more depleted melts. Since the degassing step substantially reduces the CO_2 concentration of the most enriched melts in most runs of the model, the most pronounced effect of graphite saturation is on the depleted melts. Depleted melts generated from a very reduced melting region have extremely high CO_2/Ba ratios (Figure B.3). Dissolution of CO_2 , exsolved from enriched melts, into undersaturated depleted melts will have the same qualitative effect on the CO_2 -trace element systematics.

Though graphite-saturated melting is unlikely to be important unless the mantle is significantly more reduced than indicated by $\text{Fe}^{3+}/\Sigma\text{Fe}$ ratios of Icelandic basalts (Shorttle et al., 2015), or MORB (Cottrell and Kelley, 2011; Berry et al., 2018), it is feasible that extremely high mantle CO_2 concentrations may exert an influence on redox equilibria. Whilst the CO_2 -trace element systematics of Háleyjabunga and Miðfell rule out equilibrium with graphite for most of the melting region, it is not implausible that the most extreme values of CO_2/Ba could be generated in this way. Significantly more melt inclusion analyses are required to fully characterise the high-tail of the CO_2/Ba distributions.

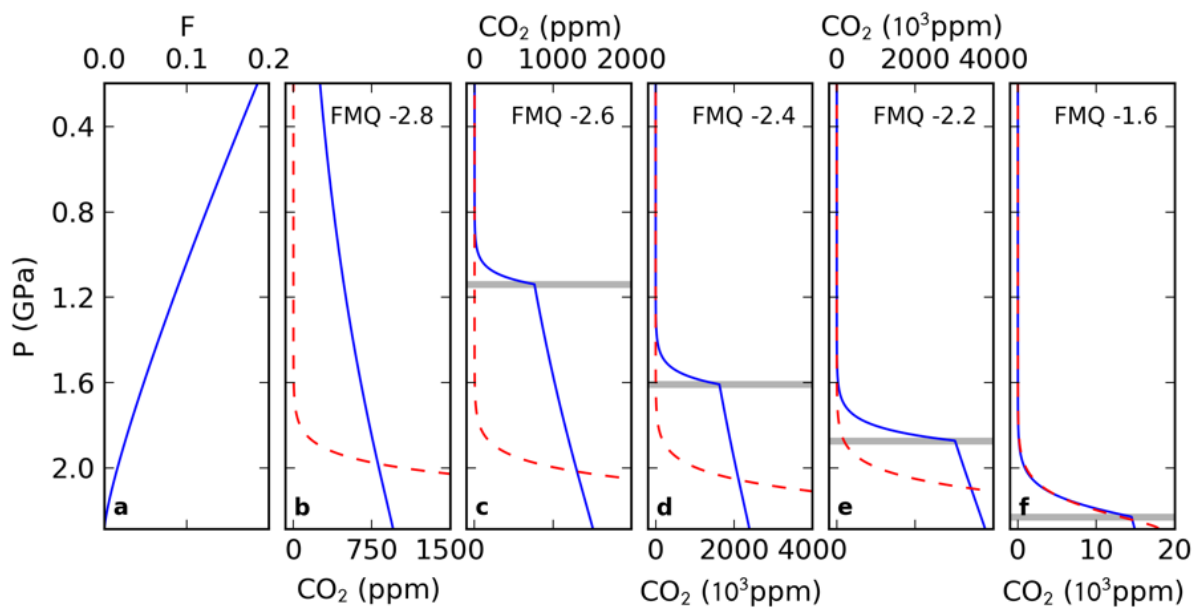


Figure B.2: Panel a shows the melt fraction as a function of pressure, calculated as described in the main text. The solid blue lines in panels b-f show the calculated CO₂ concentration of melts generated at variable oxygen fugacity, buffered relative to the FMQ buffer. Below the grey line the mantle is graphite saturated. The red dashed line shows the concentration of CO₂ in the melts in a mantle sufficiently oxidised that graphite is never saturated during melting, i.e. the result used in the main text of this paper.

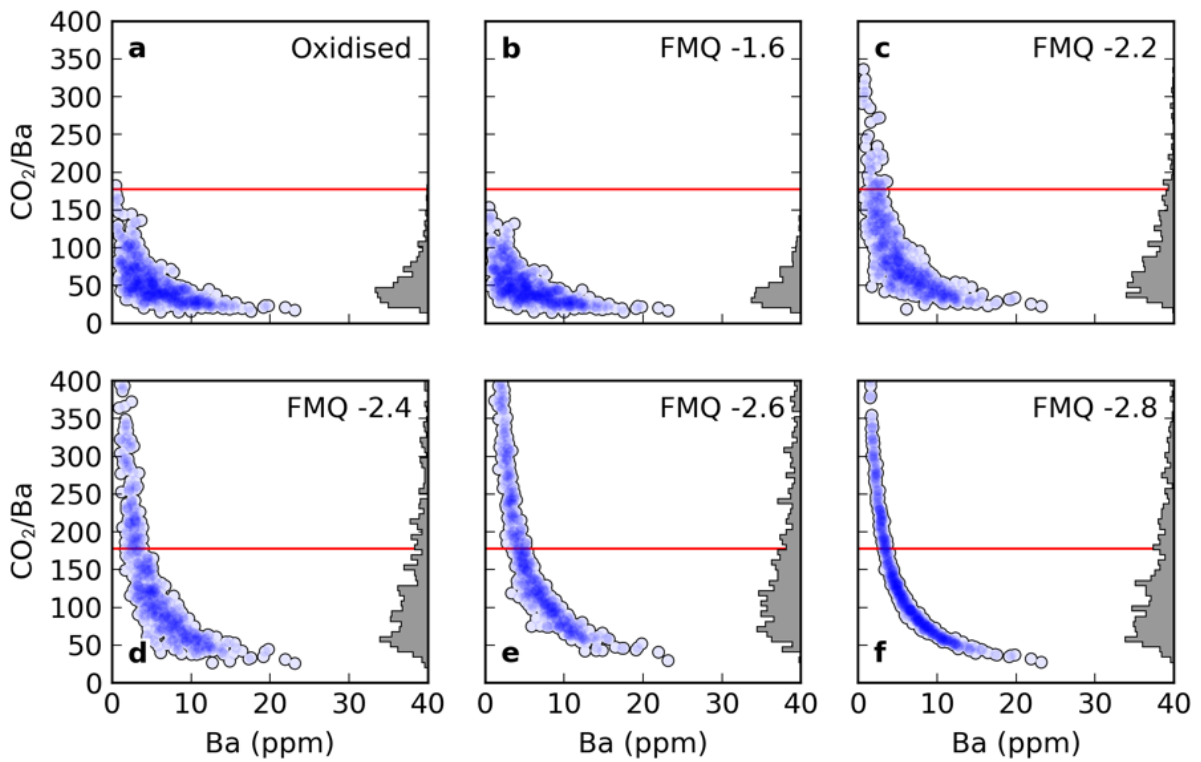


Figure B.3: Results of the mixing and degassing model for melts produced during graphite saturated melting (Error! Reference source not found.) and degassing at 2000 bar. The horizontal red and green lines show the source CO₂/Ba ratio, and the ratio inferred from orthogonal-distance regression, respectively. The shading shows the degree of CO₂ undersaturation in bars, at the pressure of degassing